Electrochemical and theoretical study of nickel(II) containing different 2,2':6',2''-terpyridines

N.G.S. Mateyise [a,1], M.M. Conradie [a,2,*], J. Conradie [a,b,3,*]

[a] *Department of Chemistry, University of the Free State, P.O. Box 339, Bloemfontein 9300, South Africa*
[b] *UiT - The Arctic University of Norway, N-9037 Tromsø, Norway*

A B S T R A C T

A series of bis(terpyridine)nickel(II) complexes were synthesized and subjected to electrochemical (cyclic voltammetry) and theoretical (using density function theory, DFT) studies. DFT calculations have confirmed, consistent with existing literature, that the oxidation and reduction reactions of bis(terpyridine)nickel(II) complexes are centered on nickel and the terpyridine ligand, respectively. Upon oxidation of the pseudo-octahedral Ni(II) complex, large changes in Ni-N bonds occur since a Jahn-Teller distorted Ni(III) complex is formed, leading to a quasi-reversible Ni(II/III) oxidation process. Conversely, small geometric changes observed during the reduction of bis(terpyridine)nickel(II) suggest a reversible process, as experimentally observed. The second reduction is quasi-reversible and is attributed to the instability of the neutral bis(terpyridine)nickel complex containing two tpy ligand radicals.

The nature of the substituents on the terpyridine ligand, characterized by Hammett constants, influences the redox potentials. These shifts result in linear relationships between the experimental redox potentials and Hammett constants, as well as DFT-calculated potentials, energies and charges associated with the specific redox process.

1. Introduction

Commonly employed in coordination chemistry, 2,2':6',2''-terpyridine (tpy) is an essential ligand in the production of metal-terpyridine complexes due to its remarkable propensity for interacting with metals. It was first isolated as a byproduct of the oxidative coupling of pyridines using the FeCl₃ catalyst [1,2]. These complexes play a significant role in fields such as catalysis, material science and supramolecular chemistry due to their unique properties and reactivity [3]. Terpyridine nickel complexes have been reported to be able to catalyse the cross-coupling of alkyl halides with alkyl nucleophiles through putative intermediates [4]. Nickel(II) complexes containing bipyridine were tested as dye sensitizers in DSSCs, producing acceptable light harvesting, required redox potentials and sufficient charge-separated lifetime, but low photocurrents, ascribed to a short-lived excited state of the Ni(II) complex [5]. While certain nickel(II) coordination complexes demonstrate properties required for redox mediators [6–8], there is currently no assessment of polypyridine complexes of nickel [9] as redox mediators to date. The redox potential of a compound determines its capability to function as a catalyst or a redox mediator. This underscores the

necessity for an electrochemical examination of nickel complexes whose redox behavior has not been previously reported. We have previously conducted an electrochemical study on nickel-bipyridine and nickel-phenanthroline complexes [10]. However, limited electrochemical data on nickel-terpyridine complexes is available, as outlined below.

Redox-active metal–organic frameworks (MOFs) and coordination polymers (CPs) such as those containing Cd(II) [11,12], Mn(II) [13], and Ni(II) [14] have extensive applications in electrocatalysis. For example, the Ni(II) polypyridine CP {[Ni(bipy)₃(H₂O)₂](bipy)(ClO₄)₂} was directly utilized as an oxygen evolution reaction catalyst in alkaline solution [14].

In 1977 the oxidation and reduction of some polypyridine complexes of Co(II), Fe(II) and Ni(II), including that of [Ni(tpy)₂](ClO₄)₂ is reported [15]. [Ni(tpy)₂](ClO₄)₃ with Ni in the +3 oxidation state is for the first time prepared and isolated using controlled potential electrolysis.

In 1992 Arna and coworkers found that some Co(II), Fe(II) and Ni(II) containing terdentate ligands to be especially active in the electrocatalytic reduction of carbon dioxide [16]. This report included the oxidation and reduction of [Ni(tpy)₂](PF₆)₂ and [Ni(vinyl-tpy)₂](PF₆)₂
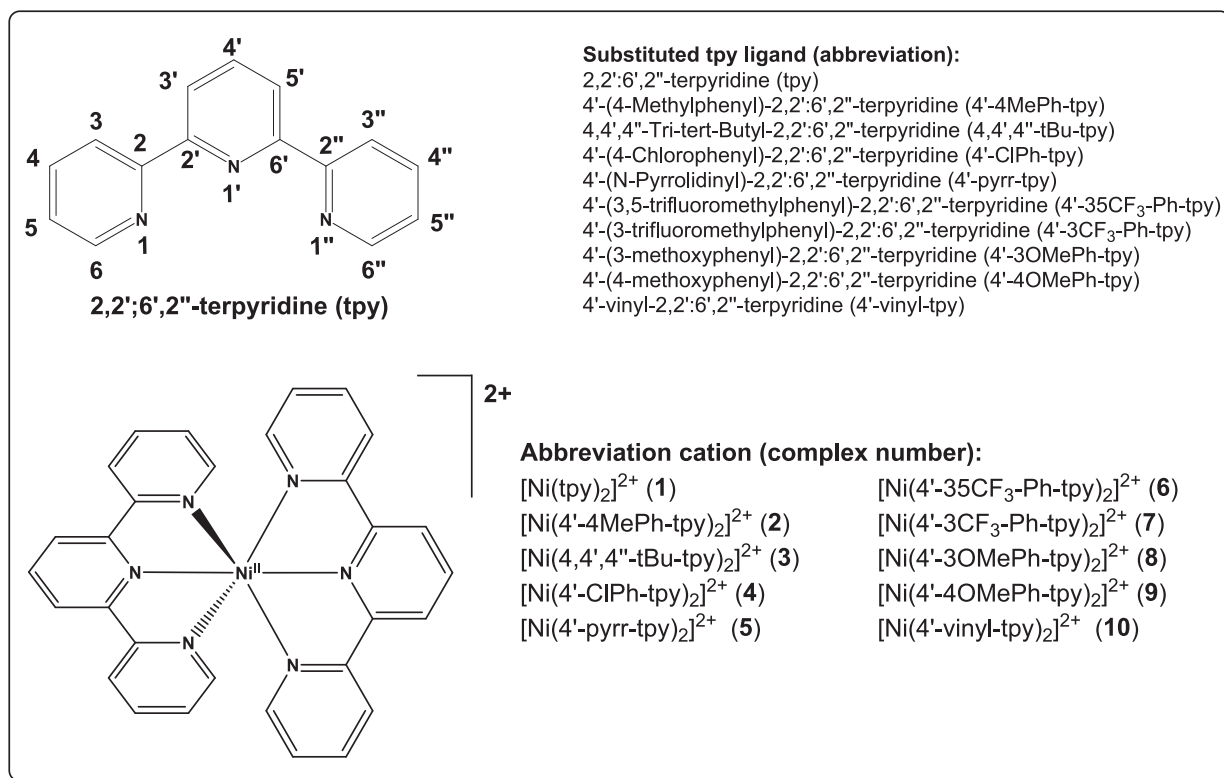

Scheme 1. The configuration of ligands and complexes in this investigation, encompassing the abbreviations employed for ligands and the numbering system for complexes.
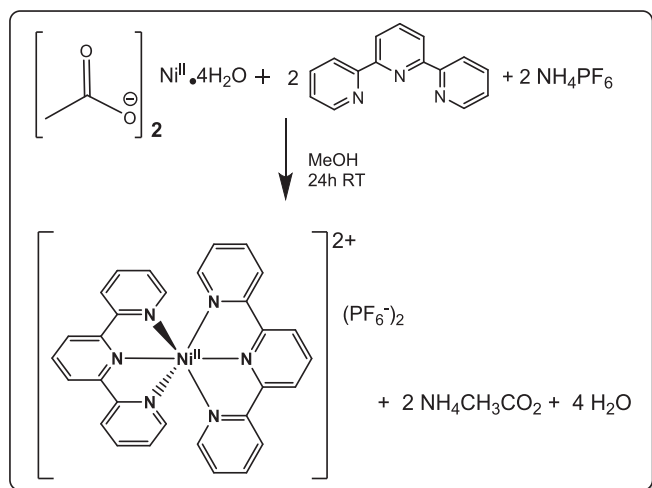
Scheme 2. Synthesis of bis(terpyridine)nickel(II) complexes.

(vinyl-tpy = 4′-vinyl-2,2′:6′,2″-terpyridine), assigning the oxidation to be metal based and the reduction ligand based. As a continuation of the previous study, research involved investigating the electrocatalytic reduction of carbon dioxide and dioxygen using electropolymerized films composed of vinyl-terpyridine complexes of Co(II), Fe(II), and Ni (II), followed [17]. More studies to reduce carbon dioxide to carbon monoxide followed. In 2014 Elgrishi used [Ni(tpy)$_2$][PF$_6$]$_2$ as
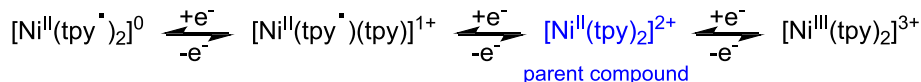
electrocatalyst for the photocatalytic reduction of carbon dioxide to carbon monoxide [18]. In addition cyclic voltammetry experiments, done in DMF/H$_2$O (95:5, v:v) of [Ni(tpy)$_2$](PF$_6$)$_2$ were reported, showing two electrochemical and chemical reversible diffusion controlled reductions at −1.62 and −1.88 V versus the ferricinium/ferrocene (Fc$^+$/Fc) redox couple. In 2017, Kuehnel studied the electro-chemistry of the complexes, including [Ni(tpy)$_2$]$^{2+}$, in a CH$_3$CN:H$_2$O (3:1) solution to investigate their stability towards water [19]. By attaching [Ni(tpy)$_2$]$^{2+}$ to a CdS quantum dot, these catalysts exhibit activity in a solely aqueous environment and demonstrate photo-catalytic capability to reduce carbon dioxide to carbon monoxide. Thus up to 2020, redox data of only bis(terpyridine)nickel(II) containing the unsubstituted tpy ligand and vinyl-tpy were reported. In 2021, cyclic voltammograms of four more complexes containing substituted tpy li-gands, were reported [20]. These cyclic voltammograms showed three well defined redox events: one oxidation and two reduction peaks. The authors showed that all observed redox events have a linear relationship with the sum of the Hammett parameters of the 4′-phenyl substituents.

Due to limited reported redox data on bis(terpyridine)nickel(II) complexes, this work present an electrochemical study using cyclic voltammetry (CV), on the series bis(terpyridine)nickel(II) complexes (1) – (5) defined in Scheme 1. In addition, a computational chemistry study on the five complexes (1) – (5), as well as the five complexes of which the redox properties are previously reported (6) – (10) [16,20] (see Scheme 1), is presented to enrich the experimental results.

$$[Ni^{II}(tpy^{\bullet})_2]^0 \underset{-e^-}{\overset{+e^-}{\rightleftharpoons}} [Ni^{II}(tpy^{\bullet})(tpy)]^{1+} \underset{-e^-}{\overset{+e^-}{\rightleftharpoons}} [Ni^{II}(tpy)_2]^{2+} \underset{-e^-}{\overset{+e^-}{\rightleftharpoons}} [Ni^{III}(tpy)_2]^{3+}$$

parent compound

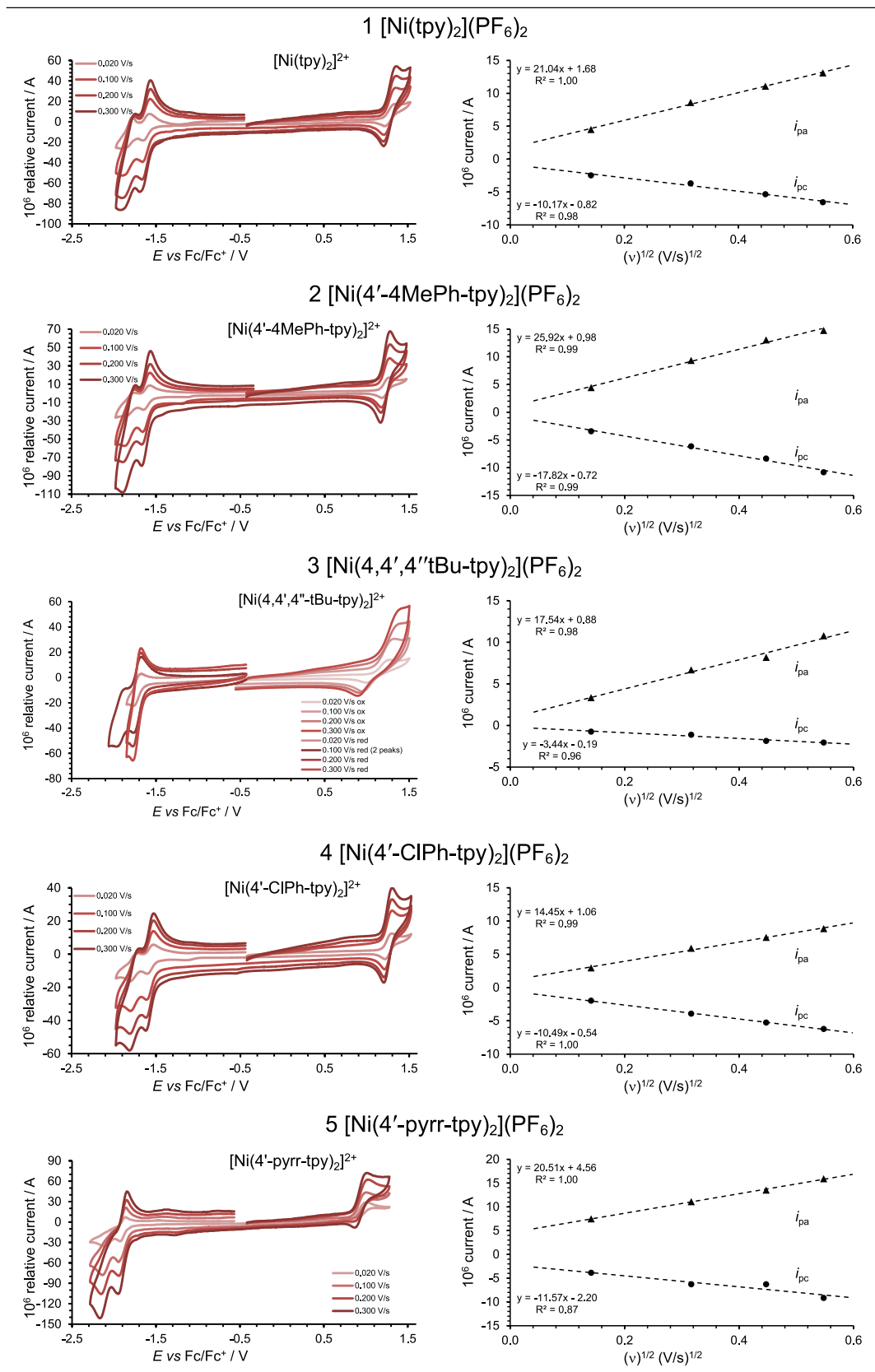**Scheme 3.** Proposed redox scheme for [Ni(tpy)$_2$]$^{2+}$.

Fig. 1. Left: Cyclic voltammograms (versus Fc/Fc$^+$) of complexes (1) – (5) in CH$_3$CN at scan rates indicated in Vs^{-1}. Right: The linear relationship between peak currents (i_p) and (scan rate)$^{1/2}$ as described by the Randles-Sevcik equation of the Ni(II/III) redox couple, of complexes (1) – (5).

Table 1

Electrochemical data (potential versus Fc/Fc$^+$) obtained at a scan rate of 0.100 Vs^{-1} in CH$_3$CN of bis(terpyridine)Ni(II/III) oxidation from this study (tw) and literature.

No	ligand	Electrolyte	$E_{1/2}$	ΔE	E_{pa}	E_{pc}	Ref
1	tpy	TBAPF$_6$	1.276	0.124	1.338	1.214	tw
	tpy[a]	TBAP[c]	1.266	0.060	1.296	1.236	[16,17]
	tpy[b]	TBAP[c]	1.218	–	–	–	[15]
2	4′-4MePh-tpy	TBAPF$_6$	1.219	0.098	1.268	1.170	tw
3	4,4′,4″-tBu-py	TBAPF$_6$	1.136	0.381	1.326	0.945	tw
4	4′-4-ClPh-tpy	TBAPF$_6$	1.257	0.084	1.299	1.215	tw
5	4′-pyrr-tpy	TBAPF$_6$	0.952	0.126	1.015	0.889	tw
6	4′-35CF$_3$-Ph-tpy	TBAPF$_6$	1.306	0.218	1.415	1.197	[20]
7	4′-3CF$_3$-Ph-tpy	TBAPF$_6$	1.264	0.107	1.318	1.211	[20]
8	4′-3OMePh-tpy	TBAPF$_6$	1.232	0.076	1.270	1.194	[20]
9	4′-4OMePh-tpy	TBAPF$_6$	1.195	0.078	1.234	1.156	[20]
10	4′-vinyl-tpy[a]	TBAP[c]	1.236	0.110	1.291	1.181	[16]

[a] Reported versus SSCE, converted to potential versus Fc/Fc$^+$ by subtracting 0.384 V as reported in [41].

[b] Reported versus SCE, converted to potential versus Fc/Fc$^+$ by subtracting 0.4156 V, obtained from $E°'$(Fc/Fc$^+$) = 0.66(5) V versus SHE in TBAPF$_6$/CH$_3$CN [42], implying $E°'$(Fc/Fc$^+$) = (0.66—0.2444) = 0.416 V versus SCE (SCE = 0.2444 V versus SHE.).

[c] TBAP = Tetra-*n*-butylammonium perchlorate.

2. Experimental

Melting points, ESI MS and UV/Vis were recorded as described in our previous works [21,22].

2.1. Synthesis of complexes (1) – (5)

Sigma-Aldrich supplied solvents and synthesis chemicals were employed without additional purification. Nickel complexes were synthesized following established literature methods as a reference [23], with minor adjustments. The desired terpyridine (1 mmol), nickel acetate tetrahydrate (0.126 g, 0.5 mmol) and ammonium hexafluorophosphate (0.163 g, 1 mmol) were all added in methanol (30 ml). The solution was stirred for 24 h at ambient temperature. The resulting off-white solution underwent filtration and was subsequently rinsed with methanol (30 ml) and H$_2$O (30 ml). The precipitate was left to air dry for 24 h to obtain the desired product as a PF$_6$ salt. Characterization data of (1) – (5) are provided below. Note, presence of the paramagnetic nickel ion causes a wide chemical shift range and broadening of all NMR signals for (1) – (5).

2.1.1. [Ni(2,2′:6′,2″-terpyridine)$_2$](PF$_6$)$_2$ (1)
Yield: 35.71 %. Colour: light yellow, M.p. 167.70 °C; UV: λ$_{max}$ 335 nm, ε$_{max}$ 28733 mol^{-1}dm^{3}cm^{-1} (CH$_3$CN). ^{1}H NMR (400 MHz, DMSO-d_6) δ 74.64, 70.01, 44.06, 18.34, 13.63, 4.11, 3.36, 3.35, 3.17. MS Calcd. [ML$_2$]$^{2+}$ (negative mode): *m/z* 524.23. Found: *m/z* 524.0. Elemental analysis calculated for NiC$_{30}$N$_6$H$_{22}$P$_2$F$_{12}$ (element, %): C, 44.20; H, 2.72; N, 10.31; obtained: C, 44.13; H, 2.65; N, 10.56.

2.1.2. [Ni(4′-(4-methylphenyl)-2,2′:6′,2″-terpyridine)$_2$](PF$_6$)$_2$ (2)
Yield: 44.32 %. Colour: Light orange, M.p. > 300 °C; UV: λ$_{max}$ 340 nm, ε$_{max}$ 31232 mol^{-1}dm^{3}cm^{-1} (CH$_3$CN). ^{1}H NMR (400 MHz, DMSO-d_6) δ 74.55, 67.29, 43.68, 13.60, 11.59, 7.04, 3.33, 0.38. MS Calcd. [ML$_2$]$^{2+}$ (negative mode): *m/z* 704.47. Found: *m/z* 704.2. Elemental analysis calculated for NiC$_{44}$N$_6$H$_{34}$P$_2$F$_{12}$ (element, %): C, 53.09; H, 3.44; N, 8.44; obtained: C, 53.01; H, 3.40; N, 8.46.

2.1.3. [Ni(4,4′,4″-tri-tert-Butyl-2,2′:6′,2″-terpyridine)$_2$](PF$_6$)$_2$ (3)
Yield: 40.19 %. Colour: Peach, M.p. 390.18 °C; UV: λ$_{max}$ 333 nm, ε$_{max}$ 24823 mol^{-1}dm^{3}cm^{-1} (CH$_3$CN). ^{1}H NMR (400 MHz, DMSO-d_6) δ 69.20, 39.42, 3.36, 2.14, 0.95. [ML$_2$]$^{2+}$ (positive mode): *m/z* 862.86. Found: *m/z* 862.4.

2.1.4. [Ni(4′-(4-Chlorophenyl)-2,2′:6′,2″-terpyridine)$_2$](PF$_6$)$_2$ (4)
Yield: 46.24 %. Colour: light orange, M.p. 136.50 °C; UV: λ$_{max}$ 341 nm, ε$_{max}$ 20941 mol^{-1}dm^{3}cm^{-1} (CH$_3$CN). ^{1}H NMR (400 MHz, DMSO-d_6) δ 73.99, 66.50, 43.70, 13.65, 11.57, 7.30, 4.11, 3.35, 3.17. Elemental analysis calculated for NiC$_{42}$N$_6$H$_{28}$Cl$_2$P$_2$F$_{12}$ (element, %): C, 48.68; H,
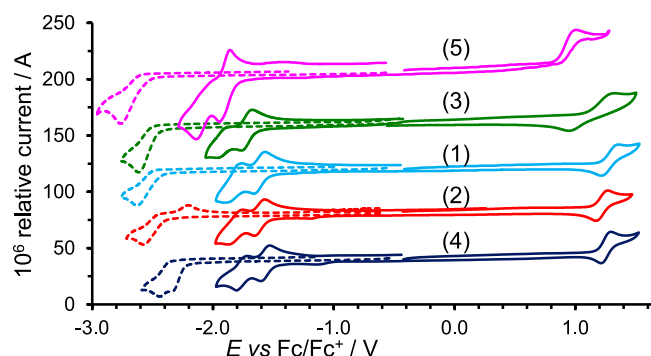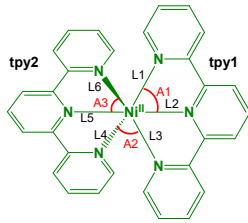

Fig. 2. Cyclic voltammograms of complexes (1) – (5) in CH$_3$CN (solid lines) and the related free uncoordinated ligands in DMF (dotted lines) at 0.100 Vs^{-1}.

Table 2

Electrochemical data (potential versus Fc/Fc$^+$) obtained at a scan rate of 0.100 Vs^{-1} of bis(terpyridine)Ni(II) reduction from this study (tw) and literature.

No		solvent	electrolyte	First reduction				Second reduction				Ref
				$E_{1/2}$	ΔE	E_{pa}	E_{pc}	$E_{1/2}$	ΔE	E_{pa}	E_{pc}	
1	tpy	CH$_3$CN	TBAPF$_6$	−1.611	0.090	−1.566	−1.656	−1.814	0.119	−1.754	−1.873	tw
	tpy[a]	CH$_3$CN	TBAP[c]	−1.584	0.080	−1.544	−1.624	−1.764	0.100	−1.714	−1.814	[16]
	tpy[b]	CH$_3$CN	TBAP[c]	−1.69								[15]
	tpy	DMF/H$_2$O (90:10)	TBAP[c]	−1.620	0.062	−1.589	−1.651	−1.880	0.065	−1.848	−1.913	[18]
	tpy	CH$_3$CN:H$_2$O (3:1)	Bu$_4$NBF$_4$	−1.58				−1.76				[19]
2	4′-4MePh-tpy	CH$_3$CN	TBAPF$_6$	−1.615	0.087	−1.571	−1.658	−1.813	0.122	−1.752	−1.874	tw
3	4,4′,4″-tBu- py	CH$_3$CN	TBAPF$_6$	−1.724	0.092	−1.678	−1.770	−2.055	0.082	−2.014	−2.096	tw
4	4′-4-ClPh-tpy	CH$_3$CN	TBAPF$_6$	−1.570	0.082	−1.529	−1.611	−1.752	0.102	−1.701	−1.803	tw
5	4′-pyrr-tpy	CH$_3$CN	TBAPF$_6$	−1.899	0.088	−1.855	−1.943	−2.099	0.123	−2.037	−2.160	tw
6	4′-35CF$_3$-Ph-tpy	CH$_3$CN	TBAPF$_6$	−1.489	0.072	−1.453	−1.525	−1.639	0.072	−1.603	−1.675	[20]
7	4′-3CF$_3$-Ph-tpy	CH$_3$CN	TBAPF$_6$	−1.549	0.071	−1.514	−1.585	−1.734	0.076	−1.696	−1.772	[20]
8	4′-3OMePh-tpy	CH$_3$CN	TBAPF$_6$	−1.589	0.075	−1.552	−1.627	−1.782	0.092	−1.736	−1.828	[20]
9	4′-4OMePh-tpy	CH$_3$CN	TBAPF$_6$	−1.624	0.077	−1.586	−1.663	−1.814	0.096	−1.766	−1.862	[20]
10	4′-vinyl-tpy[a]	CH$_3$CN	TBAP[c]	−1.634	0.080	−1.594	−1.674	−1.834	0.100	−1.784	−1.884	[16]

a–c See footnotes to Table 1.

Table 3

Selected experimental solid-state X-ray and B3LYP/6-311G(d,p)/def2-TZVPP solvent (CH$_3$CN) phase computed Ni-N bond lengths (L1-L6 in Å) and angles (A1-A3 in °) of bis(terpyridine)nickel(II) complexes [Ni(tpy)$_2$]$^{2+}$. Pg = symmetry point group. CSD = Cambridge Structural Database.

	Pg	A1	A2	A3	L1 (Ni-N$_{term1}$)	L2 (Ni-N$_{cent1}$)	L3 (Ni-N$_{term1}$)	L4 (Ni-N$_{term2}$)	L5 (Ni-N$_{cent2}$)	L6 (Ni-N$_{term2}$)	
Tpy ligand	**DFT solvent phase calculated values**										**Complex no.**
tpy	D_{2d}	77.4	92.8	77.4	2.160	2.032	2.159	2.159	2.032	2.160	**1**
4′-4MePh-tpy	C_1	77.2	92.8	77.2	2.164	2.027	2.164	2.164	2.027	2.164	**2**
4,4′,4″-tBu-tpy	C_s	77.1	92.9	77.2	2.158	2.030	2.158	2.159	2.029	2.159	**3**
4′-4ClPh-tpy	C_2	77.2	92.8	77.2	2.163	2.028	2.163	2.163	2.028	2.163	**4**
4′-pyrr-tpy	D_2	77.1	93.0	77.1	2.167	2.020	2.167	2.167	2.020	2.167	**5**
4′-35CF3-Ph	C_2	77.3	92.8	77.2	2.160	2.031	2.161	2.161	2.031	2.161	**6**
4′-3CF3-Ph	C_1	77.2	92.8	77.2	2.161	2.030	2.161	2.161	2.030	2.161	**7**
4′-3OMePh-tpy	C_1	77.2	92.8	77.2	2.162	2.028	2.162	2.162	2.028	2.161	**8**
4′-4OMePh-tpy	C_1	77.2	92.8	77.2	2.162	2.027	2.163	2.163	2.027	2.163	**9**
4-vinyl-tpy	C_2	77.3	92.9	77.3	2.162	2.026	2.162	2.162	2.026	2.162	**10**
	Experimental values available from CSD										**Note / CSD ref**
tpy		78.2	92.2	78.3	2.111	2.108	2.113	2.113	1.990	2.113	average 28 structures from CDS
4′-4MePh-tpy		77.7	89.0	78.1	2.134	2.003	2.128	2.134	2.000	2.125	average 2 structures from CDS
4′-3OMePh-tpy		78.1	97.6	78.0	2.109	1.999	2.117	2.117	1.998	2.124	EWUBEG
4′-4OMePh-tpy		78.1	91.4	77.8	2.107	1.981	2.105	2.112	1.988	2.117	average 4 structures from CDS
	Deviation of calculated values from available experiment[a]										
AD[b]		0.6	2.1	0.6	0.038	0.027	0.038	0.035	0.028	0.034	
MAD[c]		0.3	1.7	0.3	0.018	0.012	0.016	0.015	0.011	0.014	
	Deviation of exp average of 28 [Ni(tpy)$_2$]$^{2+}$ structures from experiment[d]										
AD[b,d]		0.4	1.2	0.4	0.010	0.009	0.009	0.008	0.006	0.008	
MAD[c,d]		0.2	0.9	0.3	0.007	0.007	0.006	0.005	0.005	0.006	

[a] Deviation of calculated from experiment for tpy, 4′-4MePh-tpy, 4′-3OMePh-tpy, 4′-4OMePh-tpy.

[b] AD = Average deviation.

[c] MAD = Mean absolute deviation.

[d] Deviation of exp average of Ni(tpy)$_2$ from 28 Ni(tpy)$_2$ experimental structures.

Table 4

B3LYP/6-311G(d,p)/def2-TZVPP solvent (CH$_3$CN) phase calculated energies (eV) of the different electronic states of [Ni(tpy)$_2$]^n, n = 0 – 3.

n	S	ΔE (eV)[a]
3	1/2	0.00
	3/2	0.73
2	0	1.25
	1	0.00
1	1/2	0.05
	3/2	0.00
0	0	0.95
	1	0.04
	2	0.00

[a] Relative energy for each n, with the lowest electronic state taken as 0.

2.72; N, 8.11; obtained: C, 48.63; H, 2.54; N, 8.02.

2.1.5. [Ni(4′-(N-Pyrrolidinyl)-2,2′:6′,2″-terpyridine)$_2$](PF$_6$)$_2$ (5)

Yield: 34.03 %. Colour: Grey, M.p. 333.49 °C; UV: λ_{max} 341 nm, ε_{max} 18752 mol^{-1}dm^{3}cm^{-1} (CH$_3$CN). ^{1}H NMR (400 MHz, DMSO-d_6) δ 72.30, 67.91, 42.65, 13.10, 3.38.

2.2. Cyclic voltammetry

CV experiments were done using a BAS100B Electrochemical Analyzer as described in our previous works [21,22]. The solvent used was CH$_3$CN containing tetrabutylammonium hexafluorophosphate (TBAFP$_6$) as supporting electrolyte.

2.3. DFT methods

Density functional theory (DFT) calculations were performed on bis(terpyridine)nickel(II) complexes (1) – (10), as well as their oxidized (Q = 3) and reduced (Q = 1) forms. The B3LYP functional, incorporating the Becke 88 exchange functional [24] along with the LYP correlation functional [25], was employed, utilizing the implementation available in the Gaussian 16 package [26]. The basis sets employed were triple-ζ basis set 6-311G(d,p) for lighter atoms (C, H, Cl, N) [27–30] and def2-TZVPP [31] for both the core and valence electrons of Ni. Optimizations were done in CH$_3$CN as solvent using the integral equation formalism polarizable continuum model (IEFPCM) [32,33]. The compound's input coordinates were generated using Chemcraft [34]. The natural bond orbital (NBO) calculations, molecular electrostatic potential (MESP) analysis, and theoretical calculation of the reduction potential, were done similar as describe in previous publications [35–37].

3. Results and discussion

The series of bis(terpyridine)nickel(II) complexes, (1) – (5) (Scheme 1) were synthesized in order to perform an electrochemical and computational chemistry study on (1) – (5). Section 3.1 will cover the synthesis, while an extensive electrochemical investigation utilizing
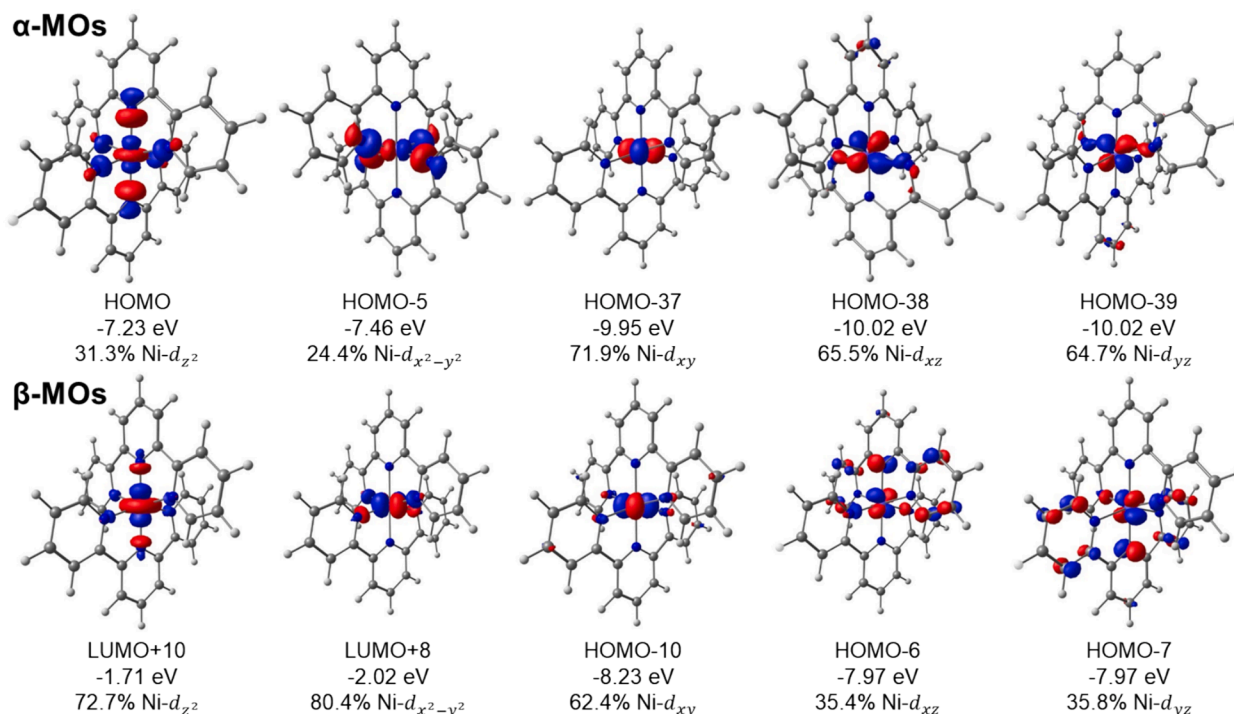
α-MOs

HOMO	HOMO-5	HOMO-37	HOMO-38	HOMO-39
-7.23 eV	-7.46 eV	-9.95 eV	-10.02 eV	-10.02 eV
31.3% Ni-d_{z^2}	24.4% Ni-$d_{x^2-y^2}$	71.9% Ni-d_{xy}	65.5% Ni-d_{xz}	64.7% Ni-d_{yz}

β-MOs

LUMO+10	LUMO+8	HOMO-10	HOMO-6	HOMO-7
-1.71 eV	-2.02 eV	-8.23 eV	-7.97 eV	-7.97 eV
72.7% Ni-d_{z^2}	80.4% Ni-$d_{x^2-y^2}$	62.4% Ni-d_{xy}	35.4% Ni-d_{xz}	35.8% Ni-d_{yz}

Fig. 3. The Ni d-based orbitals of the B3LYP/6-311G(d,p)/def2tzvpp optimized dication [Ni(tpy)$_2$]$^{2+}$. The energy and % Ni-d character of the MO are indicated. A contour level of 0.06 Åe^{-3} was employed for the MO plots. Color scheme used for atoms (online version): Ni (purple), N (blue), C (grey), and H (off-white). ((Colour online.))
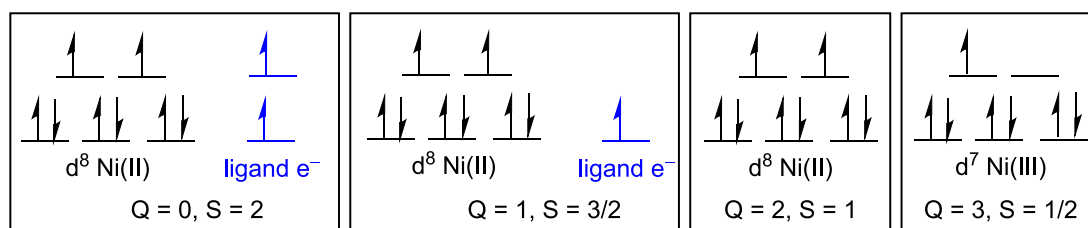
Scheme 4. Presentation of the electron occupation of the metal-d (e$_g$ top and t$_{2g}$ bottom in black) and unpaired ligand electrons (in blue) of high spin bis(terpyridine)nickel(II) ($Q = 2$) and it's oxidized ($Q = 3$) and reduced ($Q = 1$ and 0) species.
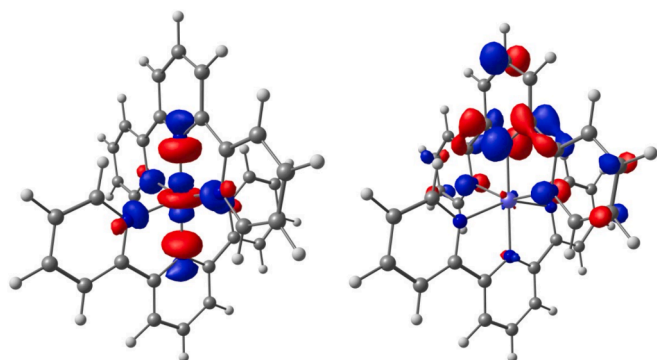
Fig. 4. The HOMO (left) and LUMO (right) of the [Ni (tpy)$_2$]$^{2+}$. A contour level of 0.06 Åe^{-3} was employed for the MO plots. Color scheme: see caption of Fig. 3.

Fig. 5. The B3LYP/6-311G(d,p)/def2tzvpp CH$_3$CN (a) optimized geometry and (b) spin density plot of [Ni(tpy)$_2$]$^{3+}$ with charge 3 and S = 1/2. The elongated bonds along the z-axis are in the vertical direction. A contour level of 0.006 Åe^{-3} was employed for the spin plot. Color scheme: see caption of Fig. 3.

cyclic voltammetry will be detailed in Section 3.2. The DFT study elucidates on the geometry, electronic structure and redox centres of (1) – (10), this is reported in section 3.3.
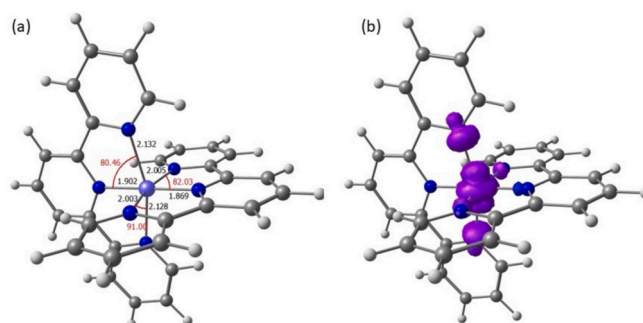
3.1. Synthesis

The synthesis scheme for bis(terpyridine)nickel(II) complexes (1) – (5) in Scheme 1 is depicted in Scheme 2. In the synthesis process, nickel
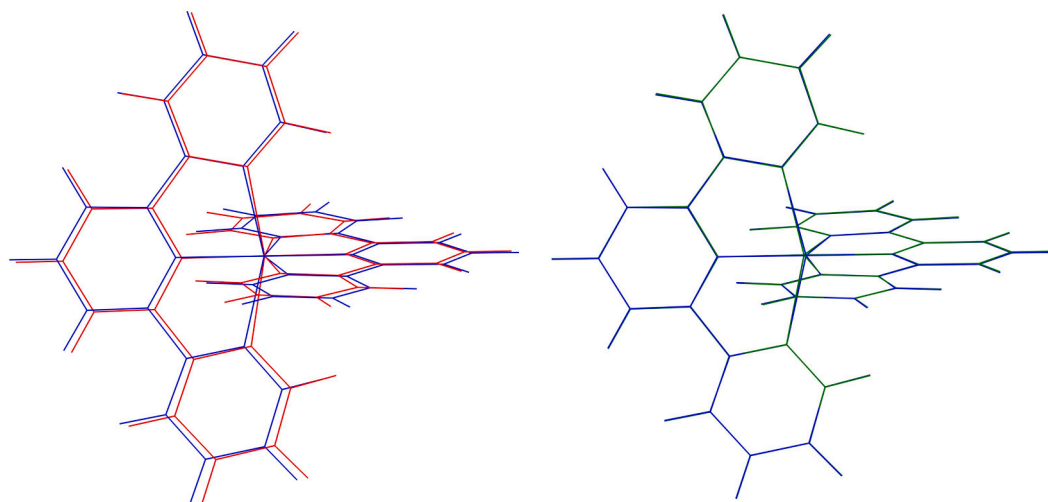
Fig. 6. Left: Overlay of B3LYP/6-311G(d,p)/def2tzvpp CH$_3$CN optimized geometry [Ni(tpy)$_2$]$^{2+}$ with $Q = 2$ in blue and $Q = 3$ in red, illustrating the reduction Ni-N bonds upon oxidation. Elongation of molecule with n = 3 is along the z-axis in the vertical direction. Right: Overlay of [Ni(tpy)$_2$]$^{2+}$ with $Q = 2$ in blue and $Q = 1$ in green, illustrating the minimal change in of the Ni-N bonds geometry upon reduction. ((Colour online.))

Table 5
B3LYP/6-311G(d,p)/def2-TZVPP solvent (CH$_3$CN) phase calculated Ni-N bond lengths (Å) of the lowest energy states of [Ni(tpy)$_2$]^n, n = 0 – 3. Bond lengths (L1 – L6) and angles (A1 – A3) are as defined in Table 3.

Q	S	A1	A2	A3	L1	L2	L3	L4	L5	L6
0	2	76.3	94.3	76.3	2.204	2.014	2.149	2.150	2.014	2.204
1	3/2	78.4	92.5	76.6	2.134	1.989	2.174	2.177	2.056	2.177
2	1	77.4	92.8	77.4	2.159	2.032	2.160	2.159	2.032	2.160
3	1/2	80.5	91.9	82.1	2.128	1.902	2.132	2.005	1.869	2.003

$Q = 2, S = 1$ $Q = 1, S = 3/2$ $Q = 0, S = 2$
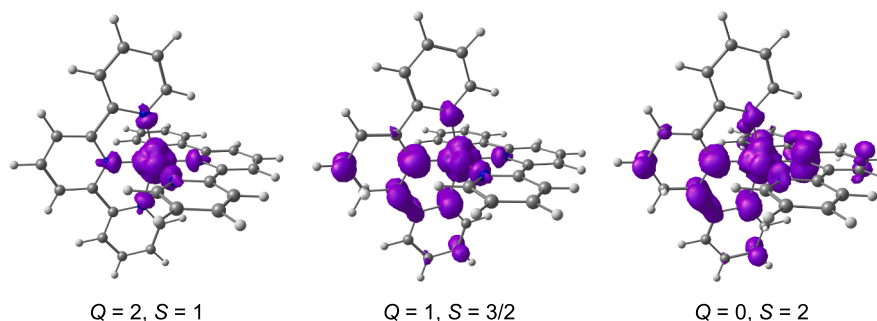
Fig. 7. Spin density plots (contour of 0.006 Åe^{-3}) of the B3LYP/6-311G(d,p)/def2tzvpp CH$_3$CN optimized geometries of bis(terpyridine)nickel with charge 2, 1 and 0. Color scheme: see caption of Fig. 3.

Table 6
Mulliken spin density on Ni and the two tpy ligands, and NBO charges on Ni of the lowest energy states of [Ni(tpy)$_2$]^n, n = 0 – 3.

Q	S	Mulliken spin density			Q$_{NBO}$
		Ni	Ligand 1	Ligand 2	Ni
0	2	1.645	1.179	1.178	0.8613
1	3/2	1.634	1.124	0.164	0.8672
2	1	1.623	0.185	0.178	0.8823
3	1/2	0.728	0.238	0.032	0.7847

acetate tetrahydrate, the desired ligand, and ammonium hexafluorophosphate were stirred at ambient temperature for 24 h. The reaction resulted in an off-white color, indicating the formation of the product. Ammonium acetate generated during the reaction was filtered out and washed with methanol and water. The resulting product was then left to air dry overnight. These outlined complexes exhibit solubility in organic solvents such as acetonitrile, DMSO, DMF, acetone, and methanol, as well as in water.

3.2. CV results

In this section, we present an electrochemical study of a series of bis (terpyridine)Ni(II) complexes (1) – (5) using CV experiments. It is worth noting that there are limited reports in the literature on the experimental electrochemical behavior of [Ni(tpy)$_2$]$^{2+}$ [15–20,38]. Most studies report that [Ni(tpy)$_2$]$^{2+}$ is reversibly being oxidized to Ni(III) and being reduced in two reversible steps. The reduction is reported to be ligand-localized [16]. DFT results, done by the group of Wieghardt in 2015, confirmed the experimental assignment [39]. Based on experimental and DFT reports, redox behaviour of [Ni(tpy)$_2$]$^{2+}$ can be described as shown Scheme 3 [38,39], where the cation and neutral complexes both
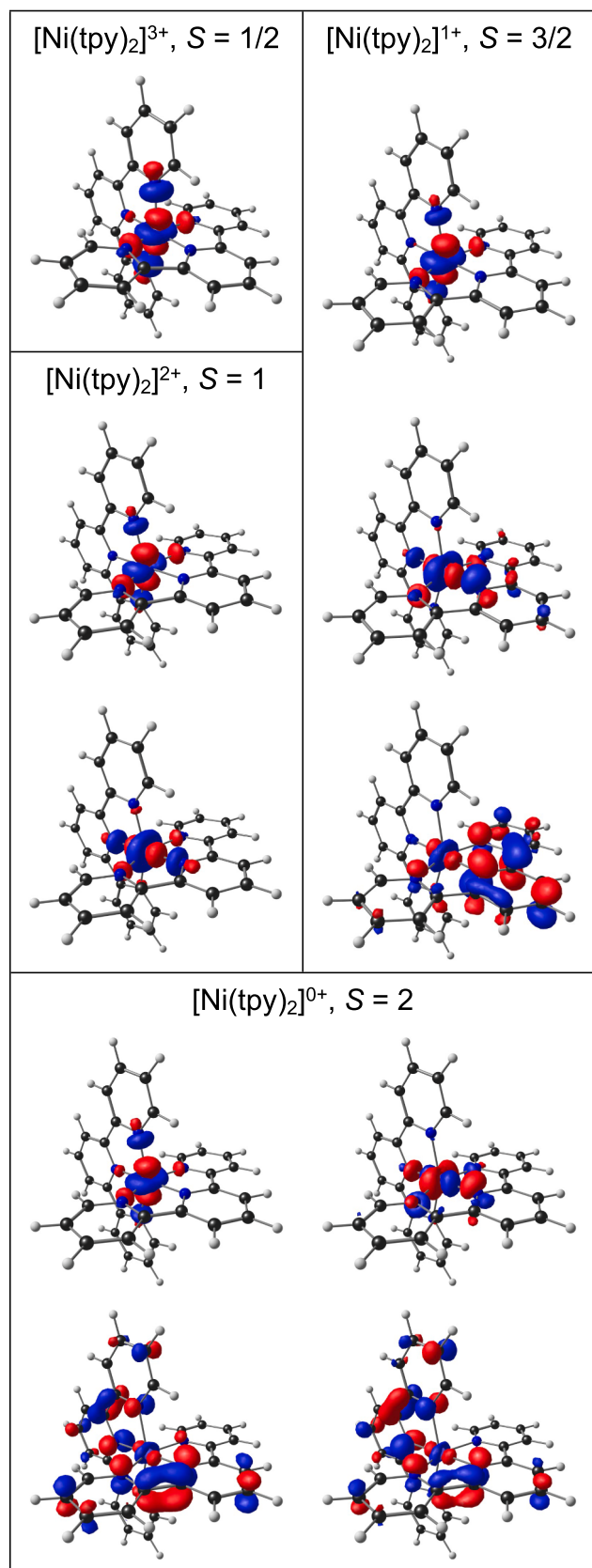
Fig. 8. Singly occupied natural orbitals of $[Ni(tpy)_2]^{n+}$ for n = 0 – 3. Color scheme: see caption of Fig. 3.

contain a nickel(II) ion coordinated to a neutral and one (tpy˙)$^{1-}$ radical anion or two radical anions, respectively.

Fig. 1 displays the cyclic voltammograms of complexes (1) – (5), each exhibiting an oxidation peak at potentials exceeding 1 V versus Fc/Fc$^+$ with notable features: large peak current potential separations (ΔE_p) and small peak current ratios (i$_{pc}$/i$_{pa}$). The Ni(II/III) redox process is thus quasi-reversible to irreversible. Complexes (2) and (4) featuring an aromatic Ph substituent group at the 4′ position of tpy, exhibits $\Delta E_p <$ 0.100 V. This observation suggests that π conjugation from the Ph substituent groups, through tpy to Ni(II), stabilizes the oxidized Ni(III)-complex more effectively compared to the other complexes. Upon oxidation, the octahedral Ni(II) complex undergoes a conversion to a Jahn-Teller distorted Ni(III) complex (refer to the discussion in section 3.3.4). While the change in geometry during oxidation may contribute to the observed large ΔE_p and small i$_{pc}$/i$_{pa}$ ratios, the $E_{1/2}$ values remain constant within 0.01 V. Furthermore, the peak currents demonstrate a direct proportionality to the square root of the scan rate, suggesting diffusion-controlled Ni(II/III) oxidation [40], see Fig. 1. Complexes containing tpy ligands with electron withdrawing substituents (pyrrole) display higher potential ($E_{1/2}$) as compare to complexes containing tpy ligands with electron donating substituents (ᵗBu, Me), see Fig. 1 and data in Table 1.

In agreement with reported data, two reduction peaks are observed for (1) – (5), see Fig. 1 with data in Table 2. Given that reduction does not entail a significant alteration in electronic structure or geometry (refer to section 3.3.5), we anticipate reversible electrochemical behavior. The first reduction exhibits $\Delta E_p <$ 0.090 V, indicating reversible electrochemical behavior.

While the two ligand based reduction peaks of (1) – (5) are between −1.5 and −2.1 V versus Fc/Fc$^+$, the reduction of the free uncoordinated ligands are more than 0.8 V lower [21], see Fig. 2.

3.3. DFT results

This section provides DFT findings for the bis(terpyridine)nickel complexes, encompassing details about the electronic structures of the molecules' ground-state geometries. The lowest energy geometries (without any imaginary frequency) and energies of the complexes were determined through DFT calculations conducted in the solvent phase (acetonitrile).

Numerous molecules of $[Ni(tpy)_2]^{2+}$, along with $[Ni(tpy)_2]^{2+}$ complexes incorporating modified terpyridine ligands, have undergone characterization through solid-state crystallography [43–45]. Nevertheless, a structural depiction of the oxidized form $[Ni(tpy)_2]^{3+}$, remains elusive [43–45]. The experimental reported ground states of $[Ni(tpy)_2]^{3+}$ and $[Ni(tpy)_2]^{2+}$ are S = ½ [46] and 1 [47] respectively. $[Ni(tpy)_2]^{1+}$ has not yet been isolated [39], while neutral $[Ni(tpy)_2]^0$ has only be proposed cyclic voltammetry experiments [39]. The group of Wieghardt [39] did a thorough study on the electronic structure of $[Ni(tpy)_2]^n$ for n = 0——3 using DFT and water as implicit solvent. They did calculations for all possible spin states of $[Ni(tpy)_2]^n$, showing that the ground state for n = 0, 1, 2 and 3 is S = 2, 3/2, 1 and ½ respectively.

3.3.1. Geometry of bis(terpyridine)nickel(II) complexes

Selected geometrical parameters of available experimental solid-state X-ray structures and our B3LYP/6-311G(d,p)/def2tzvpp calculated data of complexes (1) – (10) are provided in Table 3. Bis(terpyridine)nickel(II), (1), converged to a D_{2d} symmetry with the two central bonds shorter (Ni-N$_{cent}$, indicated as L2 and L5 as shown in Table 3) than the four terminal bonds (Ni-N$_{term}$, indicated with L1, L3, L4 and L6 as shown in Table 3). The tridentate terpyridine ligand induces strain, leading to the shorter length of the two central bonds compared to the four terminal bonds. Under D_{2d} symmetry the four terminal bonds are of equal length and the two central bonds are of equal length. The substituents on the ligands in (2) – (10) lowers the symmetry of the molecule, for example to D_2 (for 5), C_2 (for 4, 6 and 10) and C_s (for 3) or no
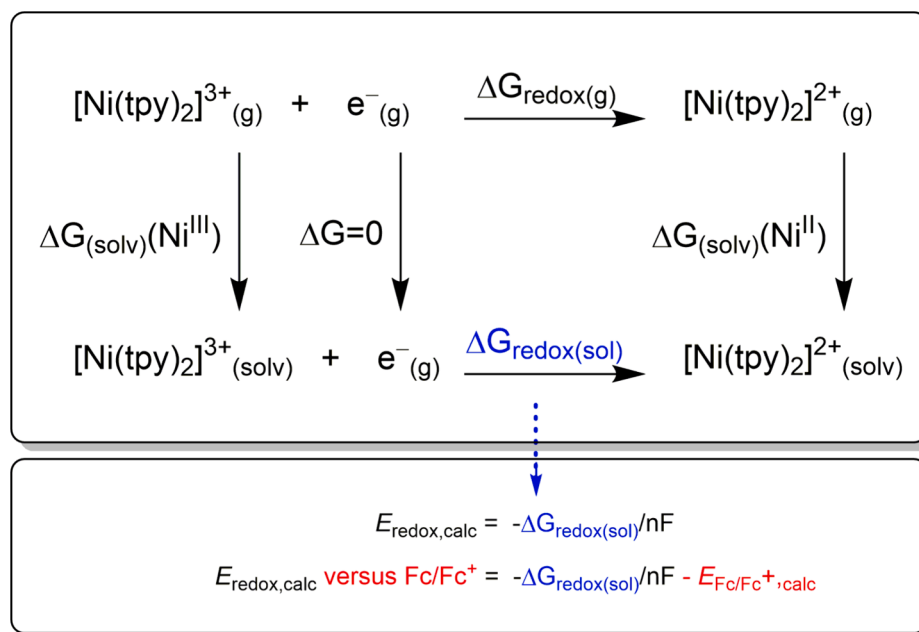
Scheme 5. Thermodynamic cycle for calculation of the absolute oxidation potential, $E_{ox,calc}$, of $[Ni(tpy)_2]^{2+}$. The cycle used for calculation of the absolute reduction potential of $[Ni(tpy)_2]^{2+}$ is similar. $\Delta G_{(g)}$ = free energy change in gas phase; $\Delta G_{(solv)}$ = solvation energy of gas phase species; $\Delta G_{ox(sol)}$ = change of free energy in solution. F = Faraday constant and n = number of transferred electrons = 1 in above scheme. For the calculated redox potential of ferrocene in acetonitrile, $E_{Fc/Fc^+,calc}$ = 4.988 V, obtained from literature [58], was used.

Table 7
DFT calculated redox potentials in CH_3CN (potential versus Fc/Fc^+) for complexes (1) – (10).

No	Ligand	E_{ox}	E_{red}
1	tpy	1.466	−1.921
2	4′-4MePh-tpy	1.406	−1.899
3	4,4′,4″-tBu- py	1.274	−2.127
4	4′-4-ClPh-tpy	1.484	−1.818
5	4′-pyrr-tpy	1.046	−2.347
6	4′-35CF$_3$-Ph-tpy	1.568	−1.700
7	4′-3CF$_3$-Ph-tpy	1.504	−1.789
8	4′-3OMePh-tpy	1.457	−1.874
9	4′-4OMePh-tpy	1.386	−1.922
10	4′-vinyl-tpy	1.402	−1.810

symmetry else. However, the Ni(tpy)$_2$ core of each molecules was still near D_{2d} symmetry, thus the length of the four terminal and of the two central bonds in each molecule were still the same within experimental error, see Table 3. The strain in the tridentate tpy ligand, causes the angles (ca 77 and 93°) in this pseudo octahedral complexes to deviate from 90° as in a real octahedron.

The computed Ni-N bond lengths of the bis(terpyridine)nickel(II) complexes are between 0.02 and 0.06 Å longer than the average experimental bond lengths for complexes (1), (2), (8) and (9) for which experimental data are available. Longer calculated Ni-N bond lengths compared to X-ray crystallography results are expected, since "chemical pressure" in the crystal decreases metal–ligand bond lengths below calculated values in gas and implicit solvent models. Thus, by obtaining slightly longer calculated bond lengths, together with the low AD and MAD values derived from the comparison between calculated and experimental structural data (Table 3), suggest that the selected DFT method is suitable for accurately describing the geometry of the bis (terpyridine)nickel(II) complex in this study.

3.3.2. Ground state of bis(terpyridine)nickel in different oxidation states

To validate the appropriateness of the chosen DFT method in accurately determining the electronic structure, energies, and the correct ground state of $[Ni(tpy)_2]^n$ for n = 0 – 3, calculations were performed for all possible spin states of $[Ni(tpy)_2]^n$. The results can be found in Table 4. The results indicate that the ground states, corresponding to the lowest energies, are S = 2, 3/2, 1, and 1/2 for n = 0, 1, 2 and 3 respectively. These findings align with available published experimental (for n = 3 [46] and n = 2 [47]) and theoretical [39] results obtained using the B3LYP functional in conjunction with water as the solvent (COSMO). The selected DFT method is, therefore, suitable for accurately determining the ground state of $[Ni(tpy)_2]^n$ for n = 0 – 3.

3.3.3. Electronic structure of bis(terpyridine)nickel(II)

This section delves into the discussion of the electronic structure, specifically the molecular orbitals (MOs), derived from DFT calculations for the bis(terpyridine)nickel(II) complex. Analyzing the character and energy of these orbitals offers valuable insights into the redox processes observed experimentally at a molecular level.

Bis(terpyridine)nickel(II) is characterized as a d^8 species with a spin state S = 1 [10,23,48]. The t_{2g} orbitals of this pseudo octahedral molecule is filled with two α unpaired electrons in the e_g orbitals, as shown in Fig. 3. The d-electron occupation of this d^8 species with S = 1 is represented as $d_{xy}^2 d_{xz}^2 d_{zy}^2 d_{x^2-y^2}^1 d_{z^2}^1$, as illustrated Scheme 4. The highest occupied MO (HOMO) is characterized by the Ni-d_{z^2} orbital as shown in Fig. 3 for (1). Similarly, the HOMOs of compounds (1) to (10) primarily reside on nickel, indicating that the oxidation process involving electron removal from the HOMO will be metal-centric, specifically Ni(II/III) oxidation. Conversely, the lowest unoccupied MOs (LUMOs) of compounds (1) to (10) are situated on the aromatic backbone of the terpyridine ligands, as exemplified by Fig. 4 for compound (1). The reduction process from (1) to (10), involving the acceptance of an electron in the LUMO, occurs on the aromatic backbone of the terpyridine ligands.

3.3.4. Bis(terpyridine)nickel(III)

Upon oxidation of bis(terpyridine)nickel(II), the bis(terpyridine) nickel(III) complex is obtained. The bis(terpyridine)nickel(III) complex is a d^7 species with spin state S = ½ [10,39,48]. After oxidation, the molecules possess 6 electrons in the t_{2g} orbital set and one unpaired
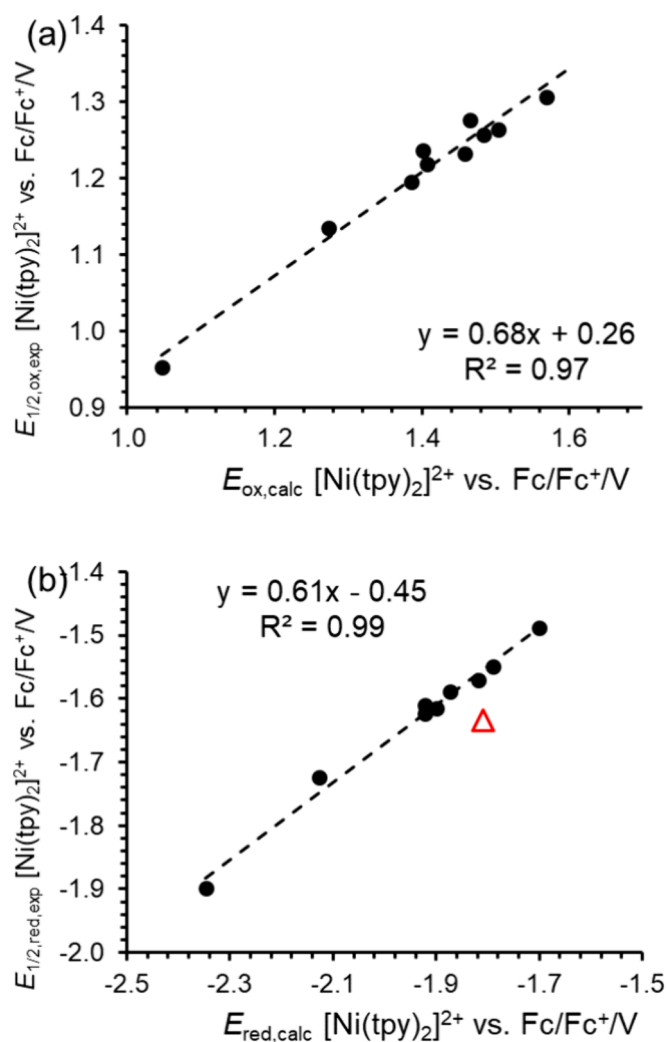
Fig. 9. Relationship involving the series of bis(tpy)-nickel(II) complexes: Experimental versus calculated redox potentials. Data of complex 10 shown with open red triangle is not included in the linear trend shown in (b). ((Colour online.))

electron in the e_g orbital set, see Scheme 4. The one unpaired electron in the e_g orbital set causes Jahn-Teller distortion in the bis(terpyridine) nickel(III) [49]. The Jahn-Teller distortion of bis(terpyridine)nickel(III), causes 2 terminal Ni-N bonds to be longer than the other 4 bonds [49]. This can be seen from the DFT optimized structure of bis(terpyridine) nickel(III) shown in Fig. 5. The longest terminal Ni-N bonds, both on the same ligand, are ca 2.13 Å, longer than the terminal bonds on the other ligand (ca 2.00 Å), confirming elongation Jahn-Teller distortion for the complex. On the other hand, the central Ni-N bonds are smaller at ca

1.90 Å. Also shown in Fig. 5 is the spin density plot of bis(terpyridine) nickel(III), showing the MO in which the one unpaired electron is located in the e_g orbital being of mainly Ni-d_{z^2} character, dictating the elongation Jahn-Teller distortion. This formulation is in agreement with oxidation of bis(terpyridine)nickel(II) being on nickel, as described in section 3.3.3. The consequence of the relatively large change on bond lengths upon oxidation, is, that the oxidation process may be slow and quasi-reversible with large peak current voltage separation, as indeed experimentally found (Table 1).

Upon oxidizing bis(terpyridine)nickel(II) to bis(terpyridine)nickel (III), all Ni-N bonds exhibit a reduction in length, as illustrated in Fig. 6 and detailed in Table 5. This phenomenon is attributed to the heightened positive charge on Ni(III), rendering it more electron-deficient compared to Ni(II). Consequently, stronger electrostatic interactions between the metal and ligands ensue, resulting in shorter Ni-N bond lengths. However, the decrease of ca 0.03 Å in the elongated Ni-N bonds of the one tpy ligand orientated along the z-axis in bis(terpyridine)nickel (III), is much smaller than the decrease of more than 0.15 Å in the terminal Ni-N bonds on the other tpy ligand, or the decrease in the central bonds of more than 0.13 Å.

3.3.5. Reduced and doubly reduced bis(terpyridine)nickel(II)

Upon the first one electron reduction of bis(terpyridine)nickel(II), $[Ni(tpy)_2]^{1+}$ with spin = 3/2 is obtained [39]. Evaluation of the spin density plot of $[Ni(tpy)_2]^{1+}$, show Mulliken spin of 1.63 e^- on Ni and 1.20 e^- on one of the tpy ligands, and only 0.16 e^- on the other tpy ligand. These values and the spin density plot of $[Ni(tpy)_2]^{1+}$ in Fig. 7 thus clearly show that this $[Ni(tpy)_2]^{1+}$ molecule can be described as containing a Ni(II) center (containing 2 unpaired electrons), one neutral tpy ligand and one tpy radical (containing 1 unpaired electron), thus $[Ni^{II}(tpy)^0(tpy\cdot)^{-1}]^{1+}$ with an electron occupation as illustrated in Scheme 4. This formulation is in agreement with the reduction of bis (terpyridine)nickel(II) being on the tpy ligand, as described in section 3.3.3. The largest change in a Ni-N bond length upon the first one electron reduction of bis(terpyridine)nickel(II), is 0.043 Å, that is much smaller than the change in Ni-N bond length upon oxidation of bis(ter-pyridine)nickel(II). Small changes in the Ni-N bonds are consistent with the central nickel being in the + 2 oxidation state. Since neither a large change in the electronic structure (no large re-arrangement of MO levels upon reduction, see Scheme 4) [50–52] or in geometry (Fig. 6 and values in Table 2) [10,21,53] does occur during the first one electron reduction process, this reduction is consistent with a reversible process, as indeed observed in section 2.2. A second reduction of bis(terpyridine)nickel(II) yields $[Ni(tpy)_2]^0$ with spin = 2 (4 unpaired electrons) and Mulliken spin of 1.64 e^- on Ni and 1.18 e^- on each of the two tpy ligands, see spin density plot in Fig. 7. The electron occupation is illustrated in Scheme 4. Comparing the Mulliken spin density on nickel of bis(terpyridine)nickel with charge 2, 1 and 0 in Table 6, it is clear that the spin on the central nickel is relatively constant, consistent with a nickel(II) center in each molecule. The spin density plots are displayed in Fig. 7.

Another confirmation that bis(terpyridine)nickel with charges 2, 1, and 0 contains a nickel(II) comes from the NBO charges on nickel in

Table 8

Hammett substituent constants (from [20,59]) and DFT solvent phase (CH_3CN) calculated energies (eV) for complexes (1) – (10).

No	Ligand	E_{HOMO}	E_{LUMO}	χ	ω	$E_{(Q=3)} - E_{(Q=2)}$	$E_{(Q=2)} - E_{(Q=1)}$	σ_{sum}
1	tpy	−7.23	−2.87	5.05	2.92	6.44	3.07	0.000
2	4′-4MePh-tpy	−6.96	−2.89	4.92	2.98	6.36	3.09	−0.050
3	4,4′,4″-tBu- py	−7.05	−2.67	4.86	2.69	6.26	2.86	−0.600
4	4′-4-ClPh-tpy	−7.17	−2.96	5.07	3.04	6.42	3.17	0.120
5	4′-pyrr-tpy	−6.41	−2.41	4.41	2.43	6.02	2.64	−0.830
6	4′-35CF$_3$-Ph-tpy	−7.30	−3.06	5.18	3.17	6.51	3.29	
7	4′-3CF$_3$-Ph-tpy	−7.25	−2.99	5.12	3.07	6.45	3.20	
8	4′-3OMePh-tpy	−6.58	−2.91	4.74	3.06	6.39	3.11	
9	4′-4OMePh-tpy	−6.50	−2.85	4.68	2.99	6.32	3.07	
10	4′-vinyl-tpy	−7.18	−2.98	5.08	3.08	6.38	3.18	−0.040

Table 9
DFT solvent phase (CH$_3$CN) calculated NBO charges Q (e$^-$) and MESP potential (au) for complexes (1) – (10).

No	Ligand	$Q_{NBO(Ni)}$	$Q_{NBO(N-average)}$	$Q_{NBO(Ni+N)}$	$V_{MESP(Ni)}$	$V_{MESP(N-average)}$	$V_{MESP(Ni+N)}$
1	tpy	0.882	−0.482	−2.008	−128.396	−18.152	−237.306
2	4′-4MePh-tpy	0.884	−0.484	−2.021	−128.406	−18.162	−237.378
3	4,4′,4″-tBu- py	0.880	−0.486	−2.035	−128.419	−18.176	−237.474
4	4′-4-ClPh-tpy	0.884	−0.483	−2.013	−128.395	−18.151	−237.304
5	4′-pyrr-tpy	0.883	−0.499	−2.111	−128.430	−18.186	−237.546
6	4′-35CF$_3$-Ph-tpy	0.884	−0.481	−2.004	−128.385	−18.141	−237.232
7	4′-3CF$_3$-Ph-tpy	0.884	−0.482	−2.006	−128.393	−18.146	−237.271
8	4′-3OMePh-tpy	0.883	−0.484	−2.018	−128.406	−18.163	−237.382
9	4′-4OMePh-tpy	0.883	−0.484	−2.018	−128.406	−18.163	−237.382
10	4′-vinyl-tpy	0.883	−0.484	−2.020	−128.402	−18.158	−237.349
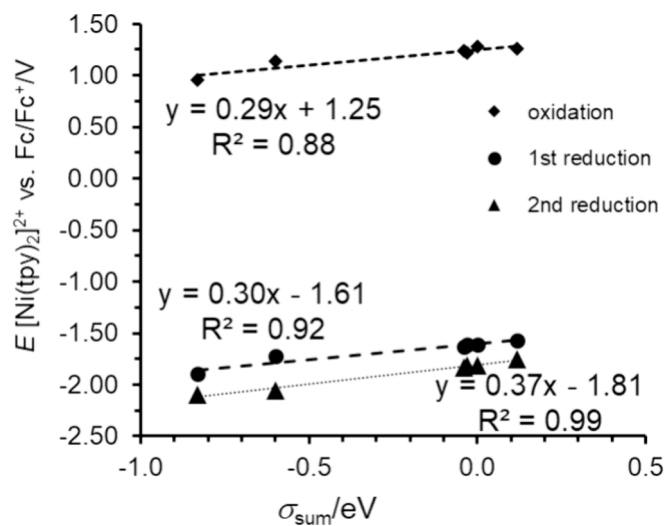
Fig. 10. Relationship between the experimental E$_{ox/red}$ and the sum of the Hammett substituent parameters on the tpy-ligand of (1) – (5), (10). Note, data points of 2 and 10 are closely overlapping, see data in Table 8.

different molecules. The NBO charge on nickel is ca 0.87 e$^-$ for bis (terpyridine)nickel with charges 2, 1, and 0 in Table 6, remaining relatively constant, consistent with a nickel(II) center in each molecule. For bis(terpyridine)nickel(III), the NBO charge on nickel is lower at 0.78 e$^-$, as expected for a more positively charged ion.

The second reduction also does not involve a large change in the arrangement of the MO levels (Scheme 4) or geometry (Table 2), though instability of the ligand based radicals that formed upon reduction (Fig. 7) could lead to quasi-reversible electrochemical behavior.

3.3.6. Natural orbitals

The concept of natural orbitals was first introduced by Löwdin in 1955 [54,55]. The natural orbitals are the eigenfunctions of the one-particle electron density matrix. In the context of DFT, the Kohn-Sham orbitals are considered as the natural orbitals. In DFT, the electronic structure of a system is described by a set of fictitious non-interacting electrons, known as Kohn-Sham electrons, moving in an effective potential. The Kohn-Sham orbitals are the orbitals associated with these Kohn-Sham electrons. The occupation numbers for these orbitals are either 2, 1, or 0, reflecting the Pauli exclusion principle, where each orbital can be occupied by up to two electrons with opposite spins [56].

In Fig. 8 the singly occupied natural orbitals of [Ni(tpy)$_2$]$^{n+}$ for n = 0 – 3 are visualized.

The assessment of the character of the singly occupied natural orbitals in [Ni(tpy)$_2$]$^{n+}$ for various charges (n = 0, 1, 2, 3) reveals distinct patterns corresponding to different spin states (S = 2, 3/2, 1, ½ respectively) and unpaired electron distributions. In the case of n = 3, one unpaired electron is localized on nickel, consistent with nickel being

in the + 3 oxidation state. For n = 2, both unpaired electrons are situated on nickel, indicating a + 2 oxidation state. When n = 1, two unpaired electrons are still found on nickel and one on a tpy ligand, suggesting a + 2 oxidation state for nickel. Finally, for n = 0, two unpaired electrons reside on nickel and two on the tpy ligands, again pointing to a + 2 oxidation state for nickel.

3.3.7. Calculation of redox potentials

In this section DFT is used to theoretically calculate the oxidation and reduction potential of bis(terpyridine)nickel(II) complexes (1) – (10). Theoretically calculated redox potentials are obtained from calculated free energy differences [35–37,57] as shown in Scheme 5. The theoretically calculated oxidation and reduction potentials of (1) – (10) are tabulated in Table 7, and compared to experimental oxidation and reduction potentials in Fig. 9. The established linear correlation between the experimentally derived redox potentials and their theoretically calculated counterparts serves as additional confirmation, reinforcing the robustness and reliability of the experimental findings. While the oxidation of (10) aligns with the observed trend, the reduction of (10) deviates from the expected pattern. It's crucial to note that the experimental data for complex (10) was collected using a different reference electrode and electrolyte compared to those employed for (1) to (9).

3.4. Combining experiment with DFT and electronic parameters

In this section DFT calculated and the Hammett substituent constants are related to the experimental redox values of bis(terpyridine)nickel(II) complexes (1) – (5). To enlarge the range of redox values, available redox values from literature of 5 more bis(terpyridine)nickel(II) complexes (complexes 6 – 10) are added to the correlations. Table 8 provide the experimental redox values, Hammett substituent constants and calculated DFT solvent phase (CH$_3$CN) energies for complexes (1) – (10), and Table 9 the DFT solvent phase (CH$_3$CN) calculated NBO charges Q (e$^-$) and MESP potential (au) for complexes (1) – (10).

3.4.1. Hammett constants

The Hammett substituent constants [59] are frequently employed in scientific literature to quantize the electronic impact of a substituent group on a phenyl or a related aromatic group within the complex to which it is bonded [60,61]. In Fig. 10, the sum of the Hammett parameters on the tpy-ligand of the series are related to the oxidation potential E$_{1/2,ox}$ and the two reduction potentials. All three trends have a good correlation factor, implying a strong linear relationship.

3.4.2. DFT energies

As outlined in section 3.3.3, the process of oxidizing a molecule entails extracting an electron from the HOMO, while reduction involves accepting an electron in the LUMO. Consequently, the ease of oxidation and reduction is directly correlated with the energy levels of the HOMO and LUMO, respectively. This relationship is illustrated in Fig. 11 for complexes (1) – (10). The oxidation potential $E_{1/2,ox}$ is directly
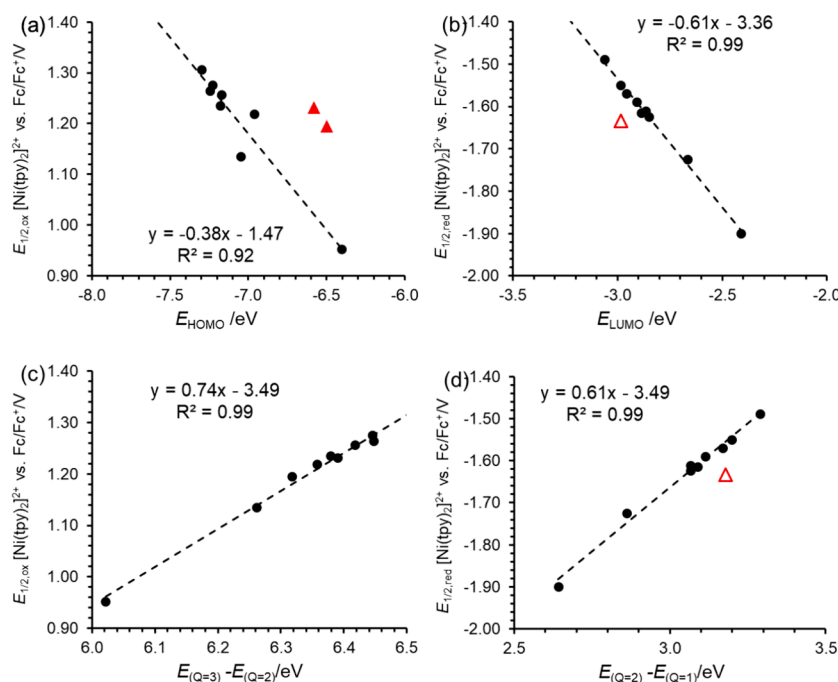
Fig. 11. Relationship involving the series of bis(tpy)-nickel(II) complexes: Between the experimental $E_{ox/red}$ and the DFT solvent phase (CH$_3$CN) calculated (a) and (b) $E_{HOMO/LUMO}$, (c) the solvent phase (CH$_3$CN) electronic energy difference of $Q = 2$ and $Q = 3$ compounds and (d) the solvent phase (CH$_3$CN) electronic energy difference of $Q = 2$ and $Q = 1$ compounds. Data of complexes 8 and 9 containing methoxy groups, shown as solid red triangles, did not fit the trend in (a), but are included in the trend (c). Data of complex 10 shown with an open red triangle deviate slightly from the trend in (b) and (d). ((Colour online.))

proportional to the energy of the HOMO, E_{HOMO}, and the reduction potential $E_{1/2,red}$ also directly proportional to the energy of the LUMO, E_{LUMO}, as displayed in Fig. 11. The oxidation of complexes (8) and (9) containing methoxy substituents, deviate from the trends. It was previously found that the redox potential of ligands containing an ester group deviate from expected relationships due to the additional effect of electron donation via lone pair resonance [62–64], that stabilizes bis (terpyridine)nickel(II), making it more difficult to oxidize at a higher than expected potential.

Oxidation in a solvent is also related to the solvent phase calculated electronic energy difference of the species involved, here the energy of the $Q = 2$ and $Q = 3$ molecules, see Fig. 11(c). (Note, solvent phase calculated electronic energy differences are used here, for the calculation of redox potentials in section 3.3.7, free energy differences was used). Similarly the reduction of a molecules in a solvent is also related to the solvent phase calculated electronic energy difference of the species involved, here the energy of the $Q = 2$ and $Q = 1$ molecules, see Fig. 11(d). Just as was found for the relationship between experimental and calculated reduction potentials in Fig. 9(b), the reduction of (10) deviates from the expected pattern in Fig. 11(b) and (d).

The initial reduction of complexes (1) – (10) involves the addition of an electron to the LUMO of bis(tpy)-nickel(II) complexes (1) – (10). This electron then occupies the HOMO of the resulting reduced species (1) – (10), specifically the series of cations, the $[Ni(tpy)_2]^{1+}$ complexes. The second reduction of complexes (1) – (10), targeting the cations of (1) – (10), involves adding an electron to the LUMO of these cations. As a result, the ease of both the first and second reductions is directly correlated with the energy levels of the HOMO and LUMO of the cations of (1) – (10), respectively. These relationships are visually represented in Fig. 12. Similar to the observations in Fig. 9(b), Fig. 11(b) and (d), the data for (10) deviates from the expected pattern in Fig. 12.

The global reactivity parameters calculated through DFT to characterize entire molecules [65] include electronegativity (χ) and the electrophilicity index (ω). This is due to the uniformity of electronegativity and electrophilicity across an atom or molecule, remaining consistent from one orbital to another within an atom or molecule [66]. The

electrophilicity index, ω, serves to quantify the electrophilic strength exhibited by atoms and molecules [67]. Molecules with higher ω values are anticipated to be more reactive towards electrophiles compared to those with lower ω values. Higher ω values are associated with complexes containing tpy ligands with electron-withdrawing substituent groups, such as Cl and CF$_3$, resulting in a higher redox potential. This correlation is illustrated in Fig. 13 (a), depicting a linear relationship between redox potentials and ω. Electronegativity, χ, measures the tendency of an atom or molecule to attract electrons towards itself [68]. Electronegativity of substituent groups influences the electronic properties of both the metal and the ligands within a molecule. Similar to ω, a higher χ value is linked to complexes that include tpy ligands with electron-withdrawing substituent groups, such as Cl and CF$_3$, leading to a higher redox potential. This association is depicted in Fig. 13 (b), demonstrating a linear relationship between redox potentials and χ.

3.4.3. DFT charges and potentials

Local reactivity parameters, such as electronic density, charges, and potentials, exhibit values that are contingent on their positions within the molecule. This characteristic enables the characterization of site-specific reactivity trends [65]. To quantify the electronic influence of various tpy substituents on nickel in compounds (1) to (10), the molecular electrostatic potential (MESP) on nickel is employed. In the literature, MESP is commonly utilized for predicting the redox potential of molecules [69–72]. In this context, both oxidation and reduction potentials are associated with the MESP on nickel and nitrogen, as illustrated in Fig. 14(a). The charges obtained through natural bond orbital (NBO) analysis offer insights into the electron distribution within the molecule, impacting both oxidation and reduction potentials. As depicted in Fig. 14(b), lower (less positive and more negative) NBO charges signify higher electron density around the nickel atom, facilitating easier electron removal from the molecule and resulting in a lower oxidation potential.
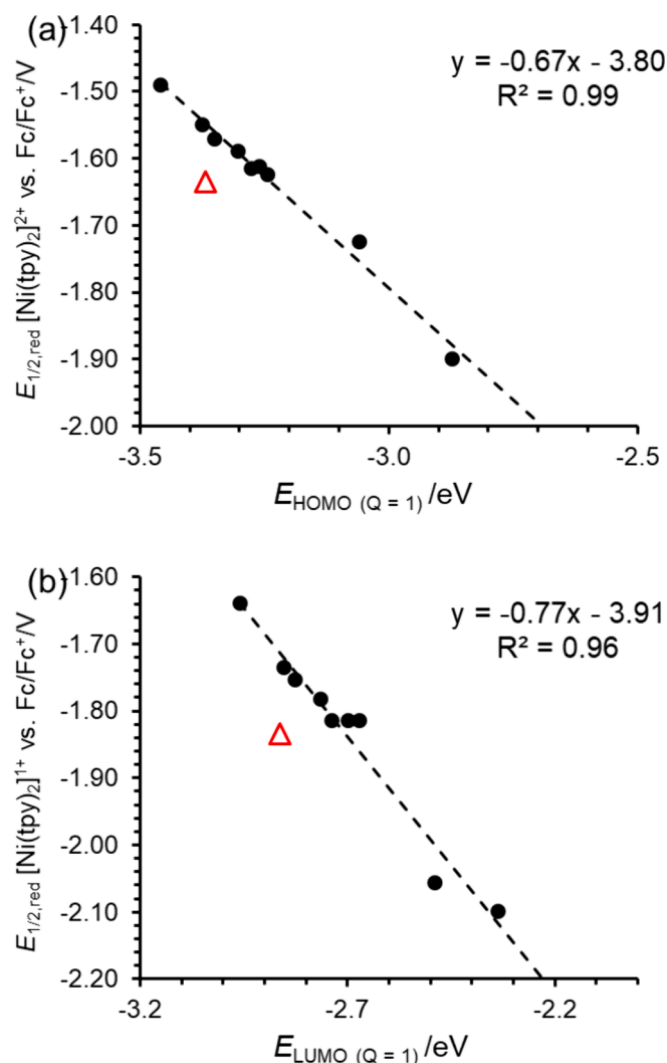
Fig. 12. Relationship involving the HOMO and LUMO energies of the series of [Ni(tpy)$_2$]$^{1+}$ complexes: experimental first and second reduction of bis(tpy)-nickel(II) (1) – (9) versus the DFT solvent phase (CH$_3$CN) calculated E_{HOMO} and E_{LUMO} respectively. Data of complex 10 shown with an open red triangle deviate from the trends. ((Colour online.))

4. Conclusions

DFT calculations confirmed, in agreement with literature, that the oxidation and reduction of bis(terpyridine)nickel(II) complexes are based on nickel and the terpyridine ligand, respectively. The Jahn-Teller distorted Ni(III) complex is formed upon oxidation of the pseudo octahedral Ni(II) complex. The significant change in Ni-N bond lengths upon oxidation, leads to slow oxidation, resulting in quasi-reversible Ni(II/III) oxidation. Small changes in the geometry upon reduction of bis(terpyridine)nickel(II) suggested reversible process, as indeed experimental observed, with the second reduction quasi-reversible ascribed to the instability of the neutral bis(terpyridine)nickel complex containing two tpy ligand radicals. The donating/withdrawing nature of the substituents, as quantified by Hammett constants, shifts the observed redox potentials to lower/higher values in such a way that linear relationships are obtained between the experimental redox potentials and Hammett constants, as well as DFT calculated potentials, energies and charges related to the specific redox process.
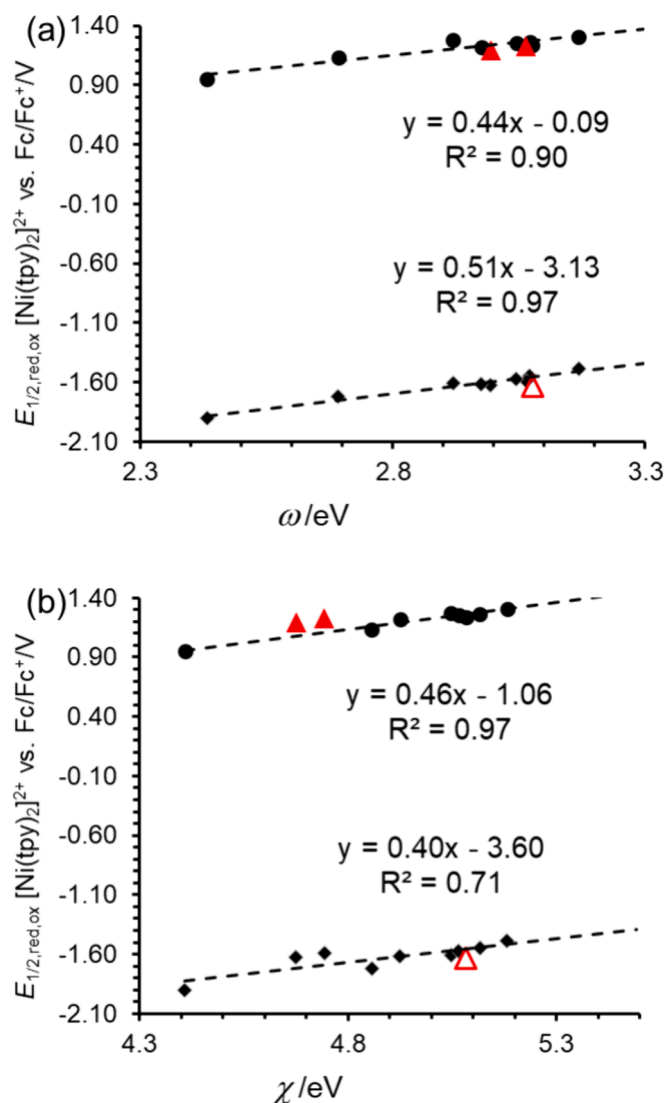

Fig. 13. Relationship involving the series of bis(tpy)-nickel(II) complexes: Between the experimental $E_{ox/red}$ and the DFT solvent phase (CH$_3$CN) calculated (a) electrophilicity index, ω, and (b) electronegativity, χ, of the molecules. Data of complexes 8 and 9 containing methoxy groups, shown as red triangles, did not fit the trends involving oxidation. Data of complex 10 shown with an open red triangle did not fit the trends involving reduction. ((Colour online.))

CRediT authorship contribution statement

N.G.S. Mateyise: Writing – review & editing, Writing – original draft, Visualization, Validation, Investigation, Formal analysis, Data curation, Conceptualization. **M.M. Conradie:** Writing – review & editing, Validation, Supervision, Resources, Funding acquisition. **J. Conradie:** Writing – review & editing, Visualization, Validation, Supervision, Software, Resources, Project administration, Methodology, Funding acquisition, Formal analysis, Data curation, Conceptualization.

Declaration of competing interest

The authors declare that they have no known competing financial interests or personal relationships that could have appeared to influence the work reported in this paper.

Data availability
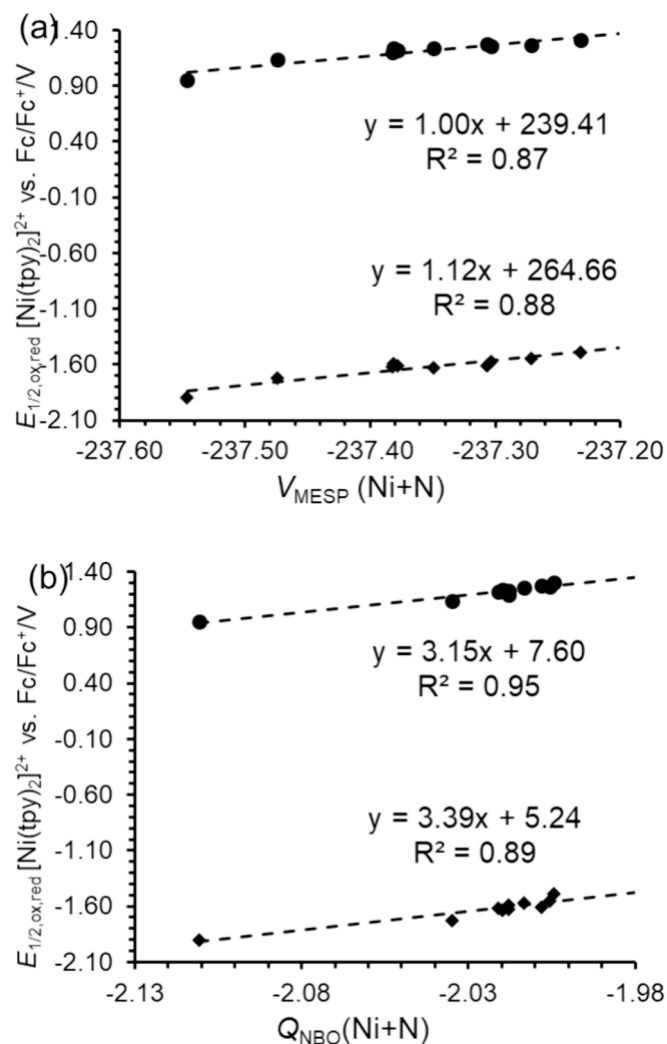
Data is within article and supporting information.

(a)

$E_{1/2, ox/red}$ [Ni(tpy)$_2$]$^{2+}$ vs. Fc/Fc$^+$/V

$y = 1.00x + 239.41$
$R^2 = 0.87$

$y = 1.12x + 264.66$
$R^2 = 0.88$

V_{MESP} (Ni+N)

(b)

$E_{1/2, ox/red}$ [Ni(tpy)$_2$]$^{2+}$ vs. Fc/Fc$^+$/V

$y = 3.15x + 7.60$
$R^2 = 0.95$

$y = 3.39x + 5.24$
$R^2 = 0.89$

Q_{NBO}(Ni+N)

Fig. 14. Relationship involving the series of bis(tpy)-nickel(II) complexes: Between the experimental $E_{ox/red}$ and the DFT solvent phase (CH$_3$CN) calculated (a) MESP potential (au) and (b) NBO charges Q (e$^-$).

Acknowledgements

Ethics statement

This work does not require any ethical statement.

Appendix A. Supplementary data

Supplementary data to this article can be found online at https://doi.org/10.1016/j.poly.2024.117075.

References

[1] G.T. Morgan, F.H. Burstall, P.A. Chloride, J. Chem. Soc. (1932) 20–30.

[2] E.U. Mughal, M. Mirzaei, A. Sadiq, S. Fatima, A. Naseem, N. Naeem, N. Fatima, S. Kausar, A.A. Altaf, M.N. Zafar, B.A. Khan, Terpyridine-metal complexes: effects of different substituents on their physico-chemical properties and density functional theory studies, R. Soc. Open Sci. 7 (2020) 201208, https://doi.org/10.1098/rsos.201208.

[3] A. Winter, U.S. Schubert, Metal-terpyridine complexes in catalytic application – A spotlight on the last decade, ChemCatChem. 12 (2020) 2890–2941, https://doi.org/10.1002/cctc.201902290.

[4] J.T. Ciszewski, D.Y. Mikhaylov, K.V. Holin, M.K. Kadirov, Y.H. Budnikova, O. Sinyashin, D.A. Vicic, Redox trends in terpyridine nickel complexes, Inorg. Chem. 50 (2011) 8630–8635, https://doi.org/10.1021/ic201184x.

[5] C.L. Linfoot, P. Richardson, K.L. McCall, J.R. Durrant, A. Morandeira, N. Robertson, A nickel-complex sensitiser for dye-sensitised solar cells, Sol. Energy. 85 (2011) 1195–1203, https://doi.org/10.1016/j.solener.2011.02.023.

[6] T.C. Li, A.M. Spokoyny, C. She, O.K. Farha, C.A. Mirkin, T.J. Marks, J.T. Hupp, Ni (III)/(IV) Bis(dicarbollide) as a fast, noncorrosive redox shuttle for dye-sensitized solar cells, J. Am. Chem. Soc. 132 (2010) 4580–4582, https://doi.org/10.1021/ja100396n.

[7] I.A. Rutkowska, A. Andrearczyk, S. Zoladek, M. Goral, K. Darowicki, P.J. Kulesza, Electrochemical characterization of Prussian blue type nickel hexacyanoferrate redox mediator for potential application as charge relay in dye-sensitized solar cells, J. Solid State Electrochem. 15 (2011) 2545–2552, https://doi.org/10.1007/s10008-011-1509-2.

[8] A.M. Spokoyny, T.C. Li, O.K. Farha, C.W. Machan, C. She, C.L. Stern, T.J. Marks, J. T. Hupp, C.A. Mirkin, Electronic tuning of nickel-based bis(dicarbollide) redox shuttles in dye-sensitized solar cells, Angew. Chemie - Int. Ed. 49 (2010) 5339–5343, https://doi.org/10.1002/anie.201002181.

[9] Y. Saygili, M. Stojanovic, N. Flores-Díaz, S.M. Zakeeruddin, N. Vlachopoulos, M. Grätzel, A. Hagfeldt, Metal coordination complexes as redox mediators in regenerative dye-sensitized solar cells, Inorganics 7 (2019) 30, https://doi.org/10.3390/inorganics7030030.

[10] Z. Mtshali, J. Conradie, Tris(polypyridine)nickel(II) complexes: Synthesis, DFT and electrochemistry, Inorganica Chim. Acta. 549 (2023) 121422, https://doi.org/10.1016/j.ica.2023.121422.

[11] C. Yang, Q. Wang, K.L. Zhang, Preparation, characterization, and electrochemical sensing performance of a novel pristine Cd-MOF and its composite with carbon nanotubes, Dalt, Trans. (2023) 5687–5703, https://doi.org/10.1039/d3dt00353a.

[12] M. Yan, T. Gu, S. Yang, K.L. Zhang, A novel hydrolytically stable fluorescent Cd(II) coordination polymer showing solvent-dependent multi-responsive fluorescence sensing to pH and some metal ions, J. Mol. Struct. 1260 (2022), https://doi.org/10.1016/j.molstruc.2022.132802.

[13] C. Yang, Y. Gu, K.L. Zhang, Proton-conductive and electrochemical-sensitive sensing behavior of a new Mn(II) chain coordination polymer, Cryst. Growth Des. 23 (2023) 704–718, https://doi.org/10.1021/acs.cgd.2c00712.

[14] T. Kumar, A. Karmakar, A. Halder, R.R. Koner, Ni(II)-based coordination polymer with Pi-conjugated organic linker as catalyst for oxygen evolution reaction activity, Energy and Fuels. 36 (2022) 2722–2730, https://doi.org/10.1021/acs.energyfuels.1c03446.

[15] R. Prasad, D.B. Scaife, Electro-oxidation and electro-reduction of some iron (II), cobalt(II) and nickel(II) polypyridyl complexes in acetonitrile, J. Electroanal. Chem. Interfacial Electrochem. 84 (1977) 373–386, https://doi.org/10.1016/S0022-0728(77)80388-4.

[16] C. Arana, S. Yan, M. Keshavarz-K, K.T. Potts, H.D. Abruna, Electrocatalytic reduction of carbon dioxide with iron, cobalt, and nickel complexes of terdentate ligands, Inorg. Chem. 31 (1992) 3680–3682, https://doi.org/10.1021/ic00043a034.

[17] C. Arana, M. Keshavarz, K.T. Potts, H.D. Abruña, Electrocatalytic reduction of CO2 and O2 with electropolymerized films of vinyl-terpyridine complexes of Fe, Ni and Co, Inorganica Chim. Acta. 225 (1994) 285–295, https://doi.org/10.1016/0020-1693(94)04059-1.

[18] N. Elgrishi, M.B. Chambers, V. Artero, M. Fontecave, Terpyridine complexes of first row transition metals and electrochemical reduction of CO 2 to CO, Phys. Chem. Chem. Phys. 16 (2014) 13635–13644, https://doi.org/10.1039/C4CP00451E.

[19] M.F. Kuehnel, K.L. Orchard, K.E. Dalle, E. Reisner, Selective photocatalytic CO 2 reduction in water through anchoring of a molecular Ni catalyst on CdS nanocrystals, J. Am. Chem. Soc. 139 (2017) 7217–7223, https://doi.org/10.1021/jacs.7b00369.

[20] J.C. Dickenson, M.E. Haley, J.T. Hyde, Z.M. Reid, T.J. Tarring, D.A. Iovan, D. P. Harrison, Fine-tuning metal and ligand-centered redox potentials of homoleptic bis-terpyridine complexes with 4'-aryl substituents, Inorg. Chem. 60 (2021) 9956–9969, https://doi.org/10.1021/acs.inorgchem.1c01233.

[21] N.G.S. Mateyise, M.M. Conradie, J. Conradie, DFT studies of the redox behavior of oligo(aza)pyridines and experimental CVs of 4'-substituted terpyridines, Results Chem. 4 (2022) 100667, https://doi.org/10.1016/j.rechem.2022.100667.

[22] N.G.S. Mateyise, M.M. Conradie, J. Conradie, Electronic effect of substituent groups on the oxidation and reduction of bis(2,2':6',2"-terpyridine)ruthenium, J. Electroanal. Chem. 947 (2023) 117807, https://doi.org/10.1016/j.jelechem.2023.117807.

[23] H. Hadadzadeh, G. Mansouri, A. Rezvani, H.R. Khavasi, B.W. Skelton, M. Makha, F. R. Charati, Mononuclear nickel(II) complexes coordinated by polypyridyl ligands, Polyhedron. 30 (2011) 2535–2543, https://doi.org/10.1016/j.poly.2011.06.037.

[24] A.D. Becke, Density-functional exchange-energy approximation with correct asymptotic behavior, Phys. Rev. a. 38 (1988) 3098–3100, https://doi.org/10.1103/PhysRevA.38.3098.

[25] C. Lee, W. Yang, R.G. Parr, Development of the Colle-Salvetti correlation-energy formula into a functional of the electron density, Phys. Rev. b. 37 (1988) 785–789, https://doi.org/10.1103/PhysRevB.37.785.

[26] M.J. Frisch, G.W. Trucks, H.B. Schlegel, G.E. Scuseria, M.A. Robb, J.R. Cheeseman, G. Scalmani, V. Barone, G.A. Petersson, H. Nakatsuji, X. Li, M. Caricato, A. V. Marenich, J. Bloino, B.G. Janesko, R. Gomperts, B. Mennucci, H.P. Hratchian, J. V. Ortiz, A.F. Izmaylov, J.L. Sonnenberg, D. Williams-Young, F. Ding, F. Lipparini, F. Egidi, J. Goings, B. Peng, A. Petrone, T. Henderson, D. Ranasinghe, V.G. Zakrzewski, J. Gao, N. Rega, G. Zheng, W. Liang, M. Hada, M. Ehara, K. Toyota, R. Fukuda, J. Hasegawa, M. Ishida, T. Nakajima, Y. Honda, O. Kitao, H. Nakai, T. Vreven, K. Throssell, J. Montgomery, J., A., J.E. Peralta, F. Ogliaro, M.J. Bearpark, J.J. Heyd, E.N. Brothers, K.N. Kudin, V.N. Staroverov, T.A. Keith, R. Kobayashi, J. Normand, K. Raghavachari, A.P. Rendell, J.C. Burant, S.S. Iyengar, J. Tomasi, M. Cossi, J.M. Millam, M. Klene, C. Adamo, R. Cammi, J.W. Ochterski, R.L. Martin, K. Morokuma, O. Farkas, J.B. Foresman, D.J. Fox, Gaussian 16, Revision B.01, (2016).

[27] A.D. McLean, G.S. Chandler, Contracted Gaussian basis sets for molecular calculations. I. Second row atoms, Z =11–18, J. Chem. Phys. 72 (1980) 5639–5648, https://doi.org/10.1063/1.438980.

[28] R. Krishnan, J.S. Binkley, R. Seeger, J.A. Pople, Self-consistent molecular orbital methods. XX. A basis set for correlated wave functions, J. Chem. Phys. 72 (1980) 650–654, https://doi.org/10.1063/1.438955.

[29] V.A. Rassolov, J.A. Pople, M.A. Ratner, T.L. Windus, 6–31G * basis set for atoms K through Zn, J. Chem. Phys. 109 (1998) 1223–1229, https://doi.org/10.1063/1.476673.

[30] J.E. Del Bene, D.H. Aue, I. Shavitt, Stabilities of hydrocarbons and carbocations. 1. A comparison of augmented 6–31G, 6–311G, and correlation consistent basis sets, J. Am. Chem. Soc. 114 (1992) 1631–1640, https://doi.org/10.1021/ja00031a015.

[31] F. Weigend, R. Ahlrichs, Balanced basis sets of split valence, triple zeta valence and quadruple zeta valence quality for H to Rn: Design and assessment of accuracy, Phys. Chem. Chem. Phys. 7 (2005) 3297, https://doi.org/10.1039/b508541a.

[32] A.V. Marenich, C.J. Cramer, D.G. Truhlar, Universal solvation model based on solute electron density and on a continuum model of the solvent defined by the bulk dielectric constant and atomic surface tensions, J. Phys. Chem. b. 113 (2009) 6378–6396, https://doi.org/10.1021/jp810292n.

[33] R.E. Skyner, J.L. Mcdonagh, C.R. Groom, T. Van Mourik, A review of methods for the calculation of solution free energies and the modelling of systems in solution, Phys. Chem. Chem. Phys. 17 (2015) 6174–6191, https://doi.org/10.1039/C5CP00288E.

[34] Chemcraft - graphical software for visualization of quantum chemistry computations., (n.d.). http://www.chemcraftprog.com/.

[35] H. Ferreira, M.M. Conradie, J. Conradie, Electrochemical and electronic properties of a series of substituted polypyridine ligands and their Co(II) complexes, Inorganica Chim. Acta. 486 (2019) 26–35, https://doi.org/10.1016/j.ica.2018.10.020.

[36] J. Conradie, Reduction potential of benzophenones, hydroxyphenones and bis(2-hydroxyphenone)copper molecules, Electrochim. Acta. 443 (2023) 141931, https://doi.org/10.1016/j.electacta.2023.141931.

[37] E. Athanasopoulos, J. Conradie, Substituent effect on the oxidation and reduction of electronically altered iron(II)-terpyridine derivatives – DFT study, Inorganica Chim. Acta. 555 (2023) 121599, https://doi.org/10.1016/j.ica.2023.121599.

[38] Y. Budnikova, D. Vicic, A. Klein, Exploring mechanisms in Ni Terpyridine Catalyzed C-C Cross-coupling reactions—A review, Inorganics. 6 (2018) 18, https://doi.org/10.3390/inorganics6010018.

[39] M. Wang, J. England, T. Weyhermüller, K. Wieghardt, Electronic structures of "low-valent" neutral complexes [NiL2]0 (S = 0; L = bpy, phen, tpy) - An experimental and DFT computational study, Eur. J. Inorg. Chem. 2015 (2015) 1511–1523, https://doi.org/10.1002/ejic.201403144.

[40] N. Elgrishi, K.J. Rountree, B.D. McCarthy, E.S. Rountree, T.T. Eisenhart, J. L. Dempsey, A practical beginner's guide to cyclic voltammetry, J. Chem. Educ. 95 (2018) 197–206, https://doi.org/10.1021/acs.jchemed.7b00361.

[41] V.V.P.A.W. Addison, V. Pavlishchuk, Conversion constants for redox potentials measured versus different reference electrodes in acetonitrile solutions at 25°C, Inorganica Chim. Acta. 298 (2000) 97–102, https://doi.org/10.1016/S0020-1693(99)00407-7.

[42] A.J.L. Pombeiro, Electron-donor/acceptor properties of carbynes, carbenes, vinylidenes, allenylidenes and alkynyls as measured by electrochemical ligand parameters, J. Organomet. Chem. 690 (2005) 6021–6040, https://doi.org/10.1016/j.jorganchem.2005.07.111.

[43] C.R. Groom, I.J. Bruno, M.P. Lightfoot, S.C. Ward, The cambridge structural database, Acta Crystallogr. Sect. B Struct. Sci. Cryst. Eng. Mater. 72 (2016) 171–179, https://doi.org/10.1107/S2052520616003954.

[44] A.G. Orpen, Applications of the cambridge structural database to molecular inorganic chemistry, Acta Crystallogr. Sect. B Struct. Sci. 58 (2002) 398–406, https://doi.org/10.1107/S0108768102002446.

[45] F.H. Allen, W.D.S. Motherwell, Applications of the Cambridge Structural Database in organic chemistry and crystal chemistry, Acta Crystallogr. Sect. B Struct. Sci. 58 (2002) 407–422, https://doi.org/10.1107/S0108768102004895.

[46] D.-Y. Noh, J.-H. Choy, Magnetic properties of nickel(III) bis(benzene-1,2-dithiolate); (n-Bu4N)[Ni(dmbit)2] and (n-Bu4N)[Ni(dmbbip)2], Synth. Met. 70 (1995) 1059–1060, https://doi.org/10.1016/0379-6779(94)02757-P.

[47] J.R. Jeitler, M.M. Turnbull, J.L. Wikaira, Synthesis, characterization and structure of transition metal complexes of 4'-methylthio-2,2': 6',2''-terpyridyl, Inorganica

[48] Chim. Acta. 351 (2003) 331–334, https://doi.org/10.1016/S0020-1693(03)00175-0.

[48] D.J. Szalda, D.H. Macartney, N. Sutin, Electron-transfer barriers and metal-ligand bonding as a function of metal oxidation state. 3. Crystal and molecular structures of tris(2,2'-bipyridine)nickel(III) triperchlorate-2-acetonitrile-0.5-dichloromethane, Inorg. Chem. 23 (1984) 3473–3479, https://doi.org/10.1021/ic00190a009.

[49] J. Conradie, Jahn-Teller distortion in bis(terpyridine)nickel(III) – elongation or compression? Results Chem. 6 (2023) 101191 https://doi.org/10.1016/j.rechem.2023.101191.

[50] J. Ferrando-Soria, O. Fabelo, M. Castellano, J. Cano, S. Fordham, H.C. Zhou, Multielectron oxidation in a ferromagnetically coupled dinickel(II) triple mesocate, Chem. Commun. 51 (2015) 13381–13384, https://doi.org/10.1039/c5cc03544a.

[51] F.P. Malan, E. Singleton, J. Conradie, M. Landman, Electrochemistry of a series of symmetric and asymmetric CpNiBr(NHC) complexes: Probing the electrochemical environment due to push-pull effects, J. Electroanal. Chem. 814 (2018) 66–76, https://doi.org/10.1016/j.jelechem.2018.02.043.

[52] B.E. Buitendach, J. Conradie, F.P. Malan, J.W. (Hans) Niemantsverdriet, J. C. Swarts, Synthesis, spectroscopy and electrochemistry in relation to DFT computed energies of ferrocene- and ruthenocene-containing beta-diketonato iridium(III) heteroleptic complexes. Structure of [(2-Pyridylphenyl)2Ir (RcCOCHCOCH3], Molecules. 24 (2019) 3923, https://doi.org/10.3390/molecules24213923.

[53] Z. Mtshali, K.G. von Eschwege, J. Conradie, Electrochemical study of the Mn(II/III) oxidation of tris(polypyridine)manganese(II) complexes, Electrochim. Acta. (2021) 138965, https://doi.org/10.1016/j.electacta.2021.138965.

[54] P.O. Löwdin, Quantum theory of many-particle systems. I. Physical interpretations by means of density matrices, natural spin-orbitals, and convergence problems in the method of configurational interaction, Phys. Rev. 97 (1955) 1474–1489, https://doi.org/10.1103/PhysRev.97.1474.

[55] V.I. Minkin, Glossary of terms used in theoretical organic chemistry (IUPAC Recommendations 1999), Pure Appl. Chem. 71 (1999) (1999) 1919–1981, https://doi.org/10.1351/pac199971101919.

[56] E.R. Davidson, Natural orbitals, Adv. Quantum Chem. 6 (1972) 235–266, https://doi.org/10.1016/S0065-3276(08)60547-X.

[57] A.V. Marenich, J. Ho, M.L. Coote, C.J. Cramer, D.G. Truhlar, Computational electrochemistry: prediction of liquid-phase reduction potentials, Phys. Chem. Chem. Phys. 16 (2014) 15068–15106, https://doi.org/10.1039/C4CP01572J.

[58] M. Namazian, C.Y. Lin, M.L. Coote, Benchmark calculations of absolute reduction potential of ferricinium/ferrocene couple in nonaqueous solutions, J. Chem. Theory Comput. 6 (2010) 2721–2725, https://doi.org/10.1021/ct1003252.

[59] C. Hansch, A. Leo, R.W. Taft, A survey of hammett substituent constants and resonance and field parameters, Chem. Rev. 91 (1991) 165–195, https://doi.org/10.1021/cr00002a004.

[60] L.P. Hammett, Some relations between reaction rates and equilibrium constants, Chem. Rev. 17 (1935) 125–136, https://doi.org/10.1021/cr60056a010.

[61] L.P. Hammett, The effect of structure upon the reactions of organic compounds. Benzene derivatives, J. Am. Chem. Soc. 59 (1937) 96–103, https://doi.org/10.1021/ja01280a022.

[62] J. Conradie, N.G.S. Mateyise, M.M. Conradie, Reduction potential of β-diketones: effect of electron donating, aromatic and ester groups, South Afr. J. Sci. Technol. 38 (2019) 1. http://www.satnt.ac.za/index.php/satnt/article/view/727.

[63] E. Chiyindiko, J. Conradie, An electrochemical and computational chemistry study of substituted benzophenones, Electrochim. Acta 373 (2021) 137894, https://doi.org/10.1016/j.electacta.2021.137894.

[64] E. Chiyindiko, E.H.G. Langner, J. Conradie, Electrochemical behaviour of 2-hydroxybenzophenones and related molecules, Results Chem. 4 (2022) 100332, https://doi.org/10.1016/j.rechem.2022.100332.

[65] J.L. Gázquez, Perspectives on the density functional theory of chemical reactivity, J. Mex. Chem. Soc. 52 (2008) 3–10, https://doi.org/10.29356/jmcs.v52i1.1040.

[66] R.G. Parr, R.A. Donnelly, M. Levy, W.E. Palke, Electronegativity: The density functional viewpoint, J. Chem. Phys. 68 (1978) 3801–3807, https://doi.org/10.1063/1.436185.

[67] R.G. Parr, L.V. Szentpály, S. Liu, Electrophilicity index, J. Am. Chem. Soc. 121 (1999) 1922–1924, https://doi.org/10.1021/ja983494x.

[68] R.S. Mulliken, A new electroaffinity scale; Together with data on valence states and on valence ionization potentials and electron affinities, J. Chem. Phys. 2 (1934) 782–793, https://doi.org/10.1063/1.1749394.

[69] B.A. Anjali, F.B. Sayyed, C.H. Suresh, Correlation and prediction of redox potentials of hydrogen evolution mononuclear cobalt catalysts via molecular electrostatic potential: A DFT study, J. Phys. Chem. A. 120 (2016) 1112–1119, https://doi.org/10.1021/acs.jpca.5b11543.

[70] B.A. Anjali, C.H. Suresh, Electronic effect of ligands vs. reduction potentials of Fischer carbene complexes of chromium: a molecular electrostatic potential analysis, New J. Chem. 42 (2018) 18217–18224, https://doi.org/10.1039/C8NJ04184A.

[71] A.A. Adeniyi, M. Landman, J. Conradie, Mo fischer carbene complexes: A DFT study on the prediction of redox potentials, J. Electrochem. Soc. 168 (2021) 066523, https://doi.org/10.1149/1945-7111/ac0a28.

[72] J. Conradie, Redox chemistry of bis(terpyridine)manganese(II) complexes – A molecular view, J. Electroanal. Chem. 913 (2022) 116272, https://doi.org/10.1016/j.jelechem.2022.116272.